Int J Earth Sci (Geol Rundsch) (2017) 106:2407–2427
DOI 10.1007/s00531-016-1436-7

ORIGINAL PAPER

Pseudo- and real-inverted metamorphism caused by the superposition and extrusion of a stack of nappes: a case study of the Southern Brasília Orogen, Brazil

Rafael Gonçalves da Motta[1] · **Renato Moraes**[1]

Received: 4 March 2016 / Accepted: 14 December 2016 / Published online: 16 January 2017

Abstract The Southern Brasília Orogen is a Neoproterozoic belt that occurs along the southernmost border of the São Francisco Craton where the Andrelândia Nappe System represents the subducted sedimentary domain and is divided into three allochthonous groups, of which the ages and *P–T* conditions of metamorphism are studied here. The basal unit, the Andrelândia Nappe, exhibits an inverted metamorphic pattern. The base of the structure, composed of staurolite, garnet, biotite, kyanite, quartz, and muscovite, marks the metamorphic peak, whereas at the top, the association of the metamorphic peak does not contain staurolite. The Liberdade Nappe, the middle unit, presents a normal metamorphic pattern; its base, close to the Andrelândia Nappe, shows paragneiss with evidence of in situ partial melting, and towards the top, coarse-grained staurolite schist is found. The staurolite-out and melt-in isograds are coincident and parallel to the main foliation. Thus, the shear zone that limits the nappes is syn-metamorphic, reheating the underlying Andrelândia Nappe and influencing the establishment of metamorphic inversion. This suggestion is supported by the monazite chemical ages, which indicates that the Andrelândia Nappe metamorphic peak (586 ± 15 Ma) is younger than that of the Liberdade Nappe (622.3 ± 7.6 Ma). The upper unit, the Serra da Natureza Klippe, bears a typical high-pressure granulite mineral assemblage that is composed of kyanite, garnet, K-feldspar, rutile, and leucosome, as well as a metamorphic peak at 604.5 ± 6.1 Ma. This tectonic assembly, with inverted and non-inverted metamorphic patterns and generation of klippen structures, is consistent with exhumation models and a strong indentor located in the lower continental crust.

Keywords Brasília Orogen · High-pressure granulite · Inverted metamorphism · Metamorphic field gradient · Monazite dating · Exhumation model

Introduction

Several major thrust zones exhibit a juxtaposition of rocks of a higher metamorphic grade over rocks of a lower grade. This configuration may indicate, but does not require, that the temperature gradients were temporarily inverted near the fault. Many examples of inverted metamorphism, where the pressure–temperature (*P–T*) conditions of rocks decrease with the structural depth, have been described, such as in the Caledonides (Andreasson and Lagerblad 1980), the Appalachians (Gibson et al. 1999), the Variscan Belt (Pitra et al. 2010), the Himalayas (Harrison et al. 1999; Mottram et al. 2014; Vannay and Grasemann 2001), and the Brasília Orogen (Garcia and Campos Neto 2003; Simões et al. 1988).

Currently, the leading model to explain extrusion and inverted metamorphism in continental collision settings is channel flow (Godin et al. 2006; Jamieson et al. 2011, 2004; Warren et al. 2008), which describes a protracted flow of a weak, viscous crustal layer between relatively rigid yet deformable bounding crustal slabs. Other models

Electronic supplementary material The online version of this article (doi:10.1007/s00531-016-1436-7) contains supplementary material, which is available to authorized users.

✉ Rafael Gonçalves da Motta
rafaelgmotta@usp.br

Renato Moraes
rmoraes@usp.br

[1] Instituto de Geociências, Universidade de São Paulo, 562, Rua do Lago-Cidade Universitária, São Paulo, SP 05508-080, Brazil

include the exhumation of rocks from the middle to the lower continental crust, either as a variation of the channel flow model with a heterogeneous or homogeneous crust (Beaumont et al. 2006) or with flow in shear zones, such as hot fold nappes-style flow (Beaumont et al. 2006; Searle and Rex 1989), or even as a ductile flow in variable-strength continental crust (Jamieson et al. 2007).

In this paper, the geology, age, *P–T* conditions, and causes of real and apparent inverted metamorphism within the Andrelândia Nappe System are presented, and a model of extrusion based on textures, thermobarometry, and in situ monazite chemical dating is proposed.

Regional geological context

The Brasilia Orogen extends to the western and southern margins of the São Francisco Craton, and was transported by a system of nappes during the Neoproterozoic. In its southern portion, it is characterized by a metamorphic stack of nappes, resulting from the collision between the San Franciscan and Paranapanema Plates (Campos Neto and Caby 1999). It is also referred to as the Southern Brasília Orogen in its southernmost portion (Fig. 1). During its development, a variety of tectonic settings were operating, and they are currently represented and organized by rocks in three main regional scale structures from W–SW to E–NE: the topmost is the Socorro-Guaxupé Nappe, which is composed of granulite, diatexite, metatexite, and suites of granite, and charnockite, and is characterized as the root of the magmatic arc; these rocks overthrust the Andrelândia Nappe System that is divided into three groups of nappes (Campos Neto et al. 2005), that is, the Três Pontas-Varginha Nappe and the associated klippen, Pouso Alto, Carvalhos and Serra da Natureza, the Liberdade Nappe, and the Andrelândia Nappe, also known, in its western portion, as the Carmo da Cachoeira Nappe. The Andrelândia Nappe System is composed of gneiss, pelite schist, quartzite, calc-silicate, mafic, and ultramafic rocks, metamorphosed under high *P* from amphibolite to granulite facies conditions, although lenses of retrogressed eclogite occur, separating one nappe from another. Gneiss and migmatite lenses of the infrastructure are common (Campos Neto et al. 2007; Trouw et al. 2000b). These rocks represent the sedimentary domain of subducted continental crust (Campos Neto et al. 2007). The Carrancas and Lima Duarte Nappes, which are mainly composed of quartzite and metapelite, represent the rocks deposited in a passive margin that was involved in the collisional process (Campos Neto et al. 2007).

An inverted metamorphic pattern is recognized within the Andrelândia Nappe System, where rocks of high-pressure and temperature override those of lower temperature (Campos Neto and Caby 1999, 2000; Garcia and Campos Neto 2003; Heilbron et al. 2004; Santos et al. 2004; Trouw et al. 1983, 2000a, b). The metamorphic inversion occurs not only due to the superposition of deeper rocks over shallow ones but also within some nappe stacks, and it has been shown that lower temperature rocks are disposed in the basal portion (Garcia et al. 2003).

Geology of the investigated area

The study area consists of a metamorphic pile, in which parts of three allochthons of the Andrelândia Nappe System crop out, as defined by Campos Neto et al. (2005): the Andrelândia Nappe represents the lower unit, the intermediate unit is the Liberdade Nappe, and the upper unit is the Serra da Natureza Klippe (Fig. 2a). Geometrically, they are articulated by the S_2 main foliation that runs parallel in the three structures and is defined by the metamorphic peak paragenesis (Fig. 2b–e).

The Serra da Natureza Klippe presents a tabular form with an apparent thickness of 300 m, lying over rocks of the Liberdade Nappe, which, in turn, are in lateral contact with rocks of the Andrelândia Nappe, with the foliation attitude folded in a synform structure (Fig. 2b). The Serra da Natureza Klippe consists of high-pressure granulite facies rocks, with a main paragenesis defined by orthoclase, kyanite, garnet, rutile, quartz, and melt as represented by leucosome veins; biotite and plagioclase are also present, but it is not always possible to determine if they were in solid state or even present at the metamorphic peak.

The Liberdade Nappe has an elongated structure, forming a synform trough, with a bent axis ranging from NE to NNE in its northern portion. This thrust unit of the Andrelândia Nappe and the fault zone that define their contact extend from a thrust fault to an extensive upright sinistral shear zone in the NNE direction; as the foliation is upright and the stretching lineation is strike-slip, this shear zone is considered to be a lateral ramp (Fig. 2). At the base of the Liberdade Nappe, pelite paragneiss, calc-silicate rocks, and amphibolite can be observed. The pelite paragneiss has kyanite, no staurolite, and abundant leucosome, attesting to its migmatitic character. At the top of the unit, staurolite coexists with kyanite and no leucosome is recognized. This is consistent with a normal metamorphic pattern from bottom to top.

The Andrelândia Nappe forms the bottom of the metamorphic stack and two metasedimentary units are identified in the study area: the basal Santo Antônio schist/gneiss is composed of muscovite, garnet, plagioclase, biotite, quartz, and rutile, with or without staurolite and kyanite, and it is in normal contact with the Serra da Boa Vista schist, that is, in reality, an alternation of pelite and psammite layers; the pelite layers exhibit paragenesis of

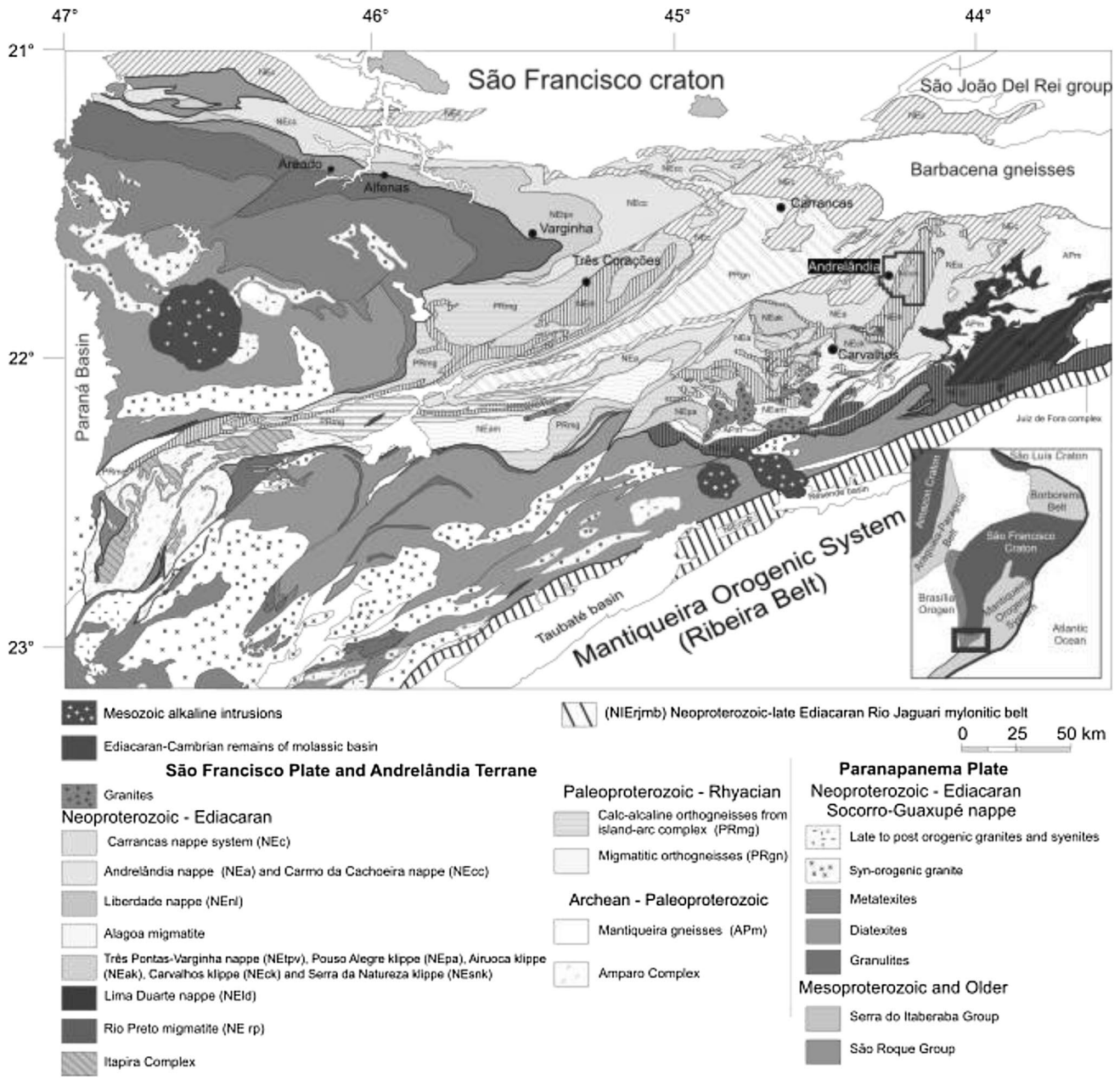

Fig. 1 Geological framework of the Southern Brasília Orogen. The *black box* indicates the study area and the location of Fig. 2. Orogen's location and its relation with Neoproterozoic Cratons are shown in the *lower right corner*

quartz, muscovite, garnet, kyanite, plagioclase, biotite, and rutile, with or without staurolite, and lenses of muscovite quartzite are interspersed. A series of repetitions of this stratigraphy can be observed within the structure, which is interpreted as caused by faults, either strike-slip or thrust faults. It is observed that near the contact between the Andrelândia and Liberdade Nappes, rocks of the former have no staurolite, which is common away from this zone.

Petrography, textural relationships, and inferred reactions

The investigation of the metamorphic mineral assemblages is first performed by comparing the minerals in different textures with reactions and divariant fields in a KFMASH petrogenetic grid drawn by Spear and Cheney (1989) and Powell et al. (1998).

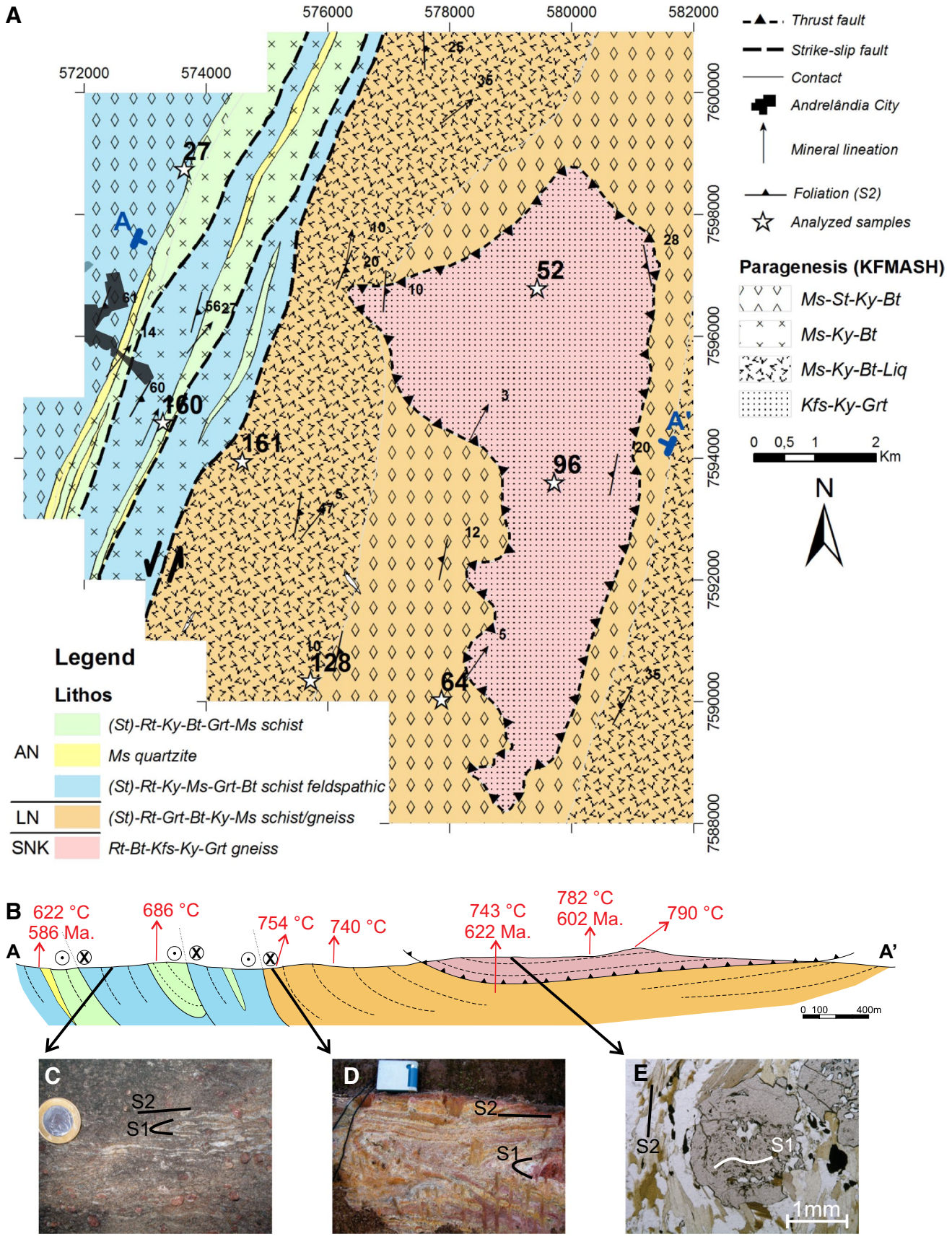
A
576000
578000
580000
582000
572000
574000
7600000
7598000
7596000
7594000
7592000
7590000
7588000
Thrust fault
Strike-slip fault
Contact
Andrelândia City
Mineral lineation
Foliation (S2)
Analyzed samples
Paragenesis (KFMASH)
Ms-St-Ky-Bt
Ms-Ky-Bt
Ms-Ky-Bt-Liq
Kfs-Ky-Grt
0 0,5 1 2
Km
N
27
160
161
52
96
64
128
Legend
Lithos
AN
(St)-Rt-Ky-Bt-Grt-Ms schist
Ms quartzite
(St)-Rt-Ky-Ms-Grt-Bt schist feldspathic
LN
(St)-Rt-Grt-Bt-Ky-Ms schist/gneiss
SNK
Rt-Bt-Kfs-Ky-Grt gneiss
B
622 °C
586 Ma.
686 °C
754 °C
740 °C
743 °C
622 Ma.
782 °C
602 Ma.
790 °C
A
A'
0 100 400m
C
S2
S1
D
S2
S1
E
S2
S1
1mm

◂**Fig. 2** **a** Geological map of the study area with isograds and metamorphic zones (UTM zone 23 S); *AN* Andrelândia Nappe, *LN* Liberdade Nappe, *SNK* Serra da Natureza Klippe. All cases of paragenesis are rutile-bearing. **b** Outcrop along *A*–*A*′. The red arrows show the approximate location of analyzed samples and their results using Zr-in-rutile thermometry and chemical ages of monazite. These data are discussed further in the text. The *black arrows* point to photos **c**–**e**, which show the S_2 main foliation in the Andrelândia Nappe, Liberdade Nappe and Serra da Natureza Klippe, respectively

The Andrelândia Nappe

In the study area, the western and basal portion of the Andrelândia Nappe crops out where the metamorphic peak paragenesis of staurolite, kyanite, garnet, muscovite, quartz, plagioclase, biotite, and rutile occurs. The chlorite inclusions in garnet porphyroblasts indicate a progressive *P*–*T* path from a temperature lower than the staurolite stability field [reaction (1)—all abbreviations after Kretz (1983)], that is, temperatures lower than 530 °C, and pressures higher than 3 kbar (Fig. 3a). This set the metamorphic peak paragenesis for the western and basal portion of the Andrelândia Nappe within the staurolite stability field, between conditions of the chlorite (reaction 2) and staurolite breakdown reactions (reaction 3).

$$\mathrm{Chl} + \mathrm{Grt} + \mathrm{Ms} \leftrightarrow \mathrm{St} + \mathrm{Bt} + \mathrm{Qtz} + \mathrm{H_2O}, \quad (1)$$

$$\mathrm{Chl} + \mathrm{St} + \mathrm{Ms} \leftrightarrow \mathrm{Bt} + \mathrm{Ky} + \mathrm{H_2O}, \quad (2)$$

$$\mathrm{St} + \mathrm{Ms} \leftrightarrow \mathrm{Grt} + \mathrm{Bt} + \mathrm{Ky} + \mathrm{H_2O}. \quad (3)$$

In the eastern and top portions of the Andrelândia Nappe, at the contact with the Liberdade Nappe, the metamorphic peak paragenesis defines the S_2 foliation, consisting of kyanite, garnet, muscovite, quartz, plagioclase, biotite, and rutile, and is staurolite-free (Fig. 3b). This indicates an inverted metamorphic pattern inside of this structure, as at its top, rocks of the Andrelândia Nappe crossed the upper limit of the staurolite stability field (reaction 3) with conditions above 650 °C.

The intergrowths of biotite and sillimanite at the garnet rims, interpreted as formed by decompression and cooling after the metamorphic peak, as well as garnet and staurolite partially replaced by chlorite, are evidence of retrometamorphism. Thus, a clockwise *P*–*T* path is inferred for the two portions of the structure, with progression from chlorite to staurolite + the kyanite field, reaching the metamorphic peak by the presence of biotite, kyanite, and garnet, without staurolite. This condition was attained only at the top of the structure, followed by a decompression stage, defined by the presence of sillimanite and biotite and the subsequent growth of chlorite.

The Liberdade Nappe

Two metamorphic zones occur inside the Liberdade Nappe. The top mineral assemblage is composed of quartz, garnet, kyanite, staurolite, muscovite, biotite, and rutile, whereas the basal portion has the addition of leucosome, but is devoid of K-feldspar and staurolite, indicative of anatexis (Fig. 3c). This suggests the breakdown of staurolite (reaction 3), followed by the incongruent melting of muscovite and plagioclase in the presence of water and inside the kyanite stability field via reaction (4):

$$\mathrm{Qtz} + \mathrm{Ms} + \mathrm{Ab} + \mathrm{H_2O} \leftrightarrow \mathrm{Ky} \pm \mathrm{Bt} + \mathrm{M}. \quad (4)$$

This implies minimum conditions of 680 °C and 7.5 kbar, that is, within the kyanite field. Amoeba-like quartz inclusions in garnet and kyanite suggest that these minerals may be the peritectic residue of the incongruent melting reaction, as previously suggested by other studies (Barbey 2007; Waters 2001). In the leucosome, some plagioclase grains present straight edges and concentric optical zoning (Fig. 3d), whereas quartz was the last phase to crystallize, as it is interstitial to other phases. Garnet corona developed around biotite, bearing several quartz inclusions with the same optical orientation. The texture also seems to be related to partial melting, as noted by other authors (Sawyer 2008; Vernon 1999). Similar textures are observed in boudins of calc-silicate and mafic rocks, as their partial melting may be facilitated by a H_2O-rich fluid influx emanating from the dehydration reactions of nearby metapsammite and metapelite, generating melt and a residual mineral association of clinopyroxene, hornblende, garnet, plagioclase, epidote, and titanite.

At the top of the Liberdade Nappe, the metamorphic peak mineral assemblage is muscovite, biotite, garnet, staurolite, kyanite, quartz, and rutile (Fig. 3e), with local inclusions of staurolite in kyanite, indicating crystallization of the latter from the former via reactions (2) and (3) (Fig. 3f). The absence of leucosome indicates that the rock did not exceed the conditions of any partial melting reaction (e.g., reaction 4), constraining the metamorphic peak conditions. Chlorite inclusions in garnet porphyroblasts suggest that the progression of metamorphism began within the chlorite stability field under *P*–*T* conditions lower than that of reaction (2). Retrometamorphism is registered by the muscovite corona, with or without staurolite, and in the presence of kyanite, which is consistent with reaction (3), from high to low temperature, implying re-hydration at temperatures below 650 °C. In some samples, only a kyanite pseudomorph is left, and because garnet is involved in this reaction as a reactant, staurolite presents a decrease in *X*Mg values at the rims. The garnet also presents signs of retrometamorphism due to the presence of biotite and chlorite at its rims. Rutile is replaced by ilmenite, following a decompression

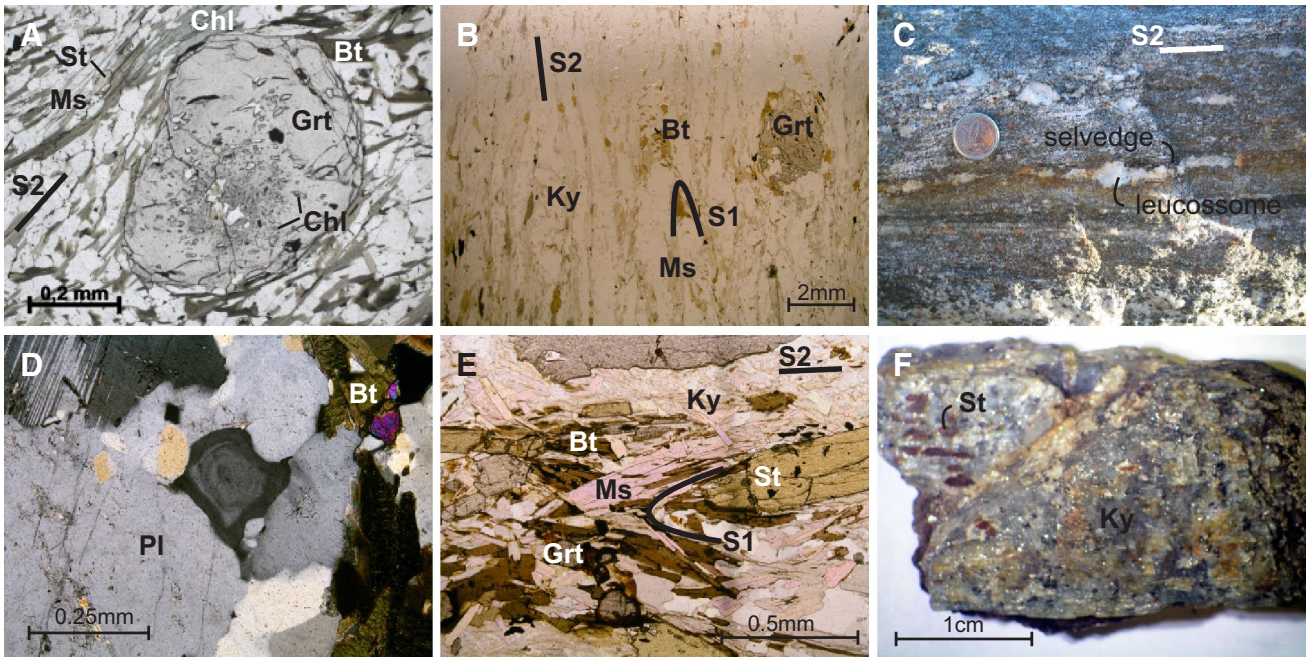

Fig. 3 **a** Staurolite–garnet–biotite–muscovite–quartz–plagioclase paragenesis with chlorite inclusion in garnet, from the base of the Andrelândia Nappe (SN-27); **b** kyanite–garnet–biotite–muscovite–quartz–plagioclase paragenesis without staurolite from the top of the Andrelândia Nappe (SN-160); **c** stromatic migmatite with biotite selvedge from the base of the Liberdade Nappe (SN-128); **d** plagioclase grain presenting straight edges and concentric chemical zoning in leucosome, Liberdade Nappe (SN-128; cross polarized light); **e** metamorphic peak paragenesis without evidence of partial melting and staurolite-bearing, top of the Liberdade Nappe (SN-64); **f** staurolite inclusions in kyanite, which indicate crystallization at the expense of staurolite, Liberdade Nappe (SN-11). All photomicrographs were taken with parallel polarized light, unless otherwise noted

path from 10 kbar, as inferred from the position of reaction (5), and experimentally calibrated (Bohlen et al. 1983) as:

$$\text{Alm} + \text{Rt} \leftrightarrow \text{Ilm} + \text{Ky} + \text{Qtz}. \quad (5)$$

In mafic and calc-silicate rocks, clinopyroxene is replaced by hornblende, which, in turn, is replaced by a greenschist facies association, with actinolite, epidote, and carbonate. Rutile is only observed as inclusions within clinopyroxene and garnet porphyroblasts, and in the matrix, only ilmenite and titanite occur. Thus, it is possible to infer a clockwise *P–T* path for the Liberdade Nappe, with progression of metamorphism from the garnet + staurolite stability field, crossing kyanite + staurolite and consumption of the latter, achieving melting reactions of muscovite, quartz, and H_2O, with or without albite at its base. The metamorphic peak is followed by a near-isothermal decompression stage, represented by biotite + plagioclase symplectite, which replaced the garnet rims in mafic and calc-silicate rocks, whereas rutile was replaced by ilmenite or titanite.

Serra da Natureza Klippe

The rocks of the Serra da Natureza Klippe have an abundant garnet and kyanite-bearing leucosome, whereas the granulite residue consists of quartz, orthoclase, garnet, kyanite, biotite, and rutile (Fig. 4a), as part of the peak mineral assemblage, for which the stability of biotite is uncertain. Staurolite is observed as inclusions in garnet (Fig. 4b), and muscovite is observed as a retrograde product of kyanite breakdown (Fig. 4c). The presence of this high-pressure granulite facies mineral assemblage defines a metamorphic jump in relation to rocks of the Liberdade Nappe and the top rocks with paragenesis, where staurolite and muscovite are stable. The absence of muscovite in the Serra da Natureza rocks indicates that the muscovite breakdown reaction crossed inside the kyanite field following reaction (6) (Vielzeuf and Holloway 1988):

$$\text{Ms} + \text{Qtz} \leftrightarrow \text{Kfs} + \text{Ky} + \text{Bt} + \text{M}. \quad (6)$$

The observed mineral assemblage is characteristic of high-pressure granulite facies, as discussed by O'Brien and Rotzler (2003). These rocks only rarely exhibit a biotite-rich melanosome as they generally consist of garnet, rutile, and kyanite, which is consistent with the biotite melting reaction crossing inside the kyanite stability field (reaction 7), with a minimum temperature of 850 °C and pressures higher than 10 kbar. The leucosome contains kyanite and garnet, both with either amoeba-like or rounded inclusions of perthite and quartz (Fig. 4d), which are interpreted,

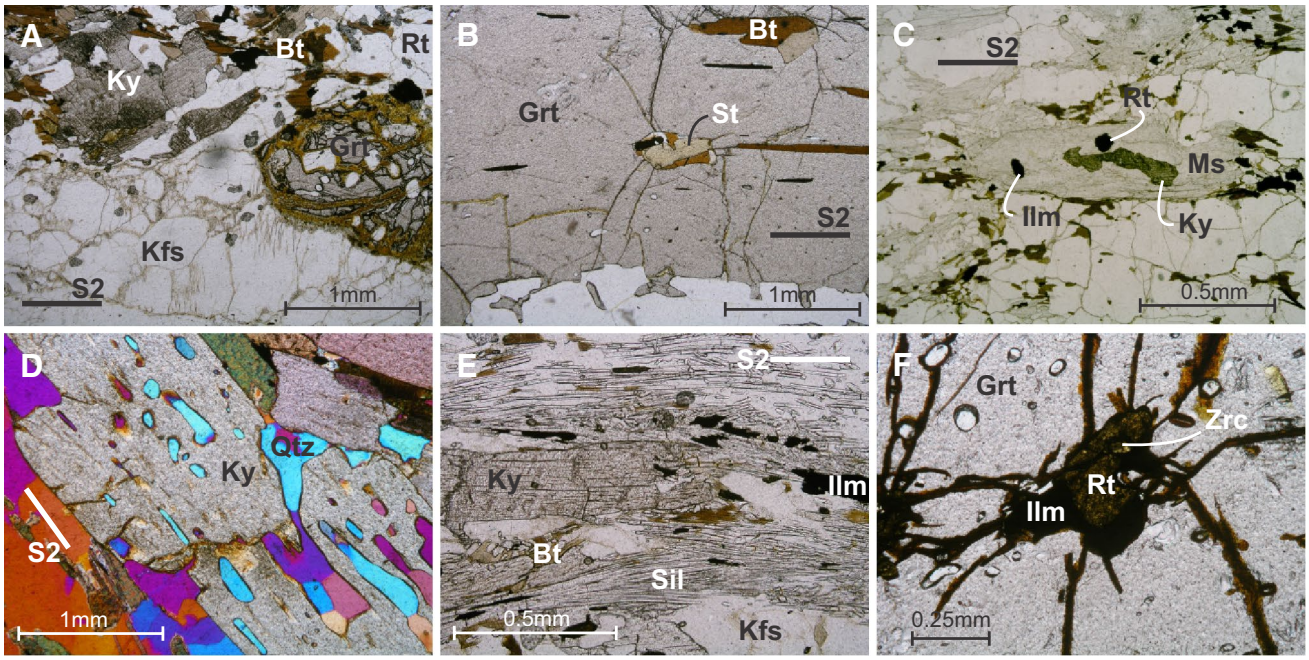

Fig. 4 **a** High-pressure granulite paragenesis with rutile–kyanite–garnet-orthoclase, Serra da Natureza Klippe (SN-99); **b** staurolite inclusion in garnet used to infer progression of metamorphism from the staurolite zone in the Serra da Natureza Klippe (SN-107); **c** amoeba-like quartz inclusions in kyanite, all with optical continuity, and leftover grains consumed during kyanite growth, Serra da Natureza Klippe (SN-96; cross polarized light and gypsum plate); **d** kyanite partially replaced by retrometamorphic skeletal intergrowth of biotite and sillimanite, Serra da Natureza Klippe (SN-69); **e** retrometamorphic replacement of kyanite by muscovite, and rutile by ilmenite, Serra da Natureza Klippe (SN-14); **f** rutile partially replaced by ilmenite and zircon along cracks inside garnet, Serra da Natureza Klippe (SN-96). All photomicrographs were taken with parallel polarized light, unless otherwise noted

respectively, as partially dissolved and peritectic phases of reaction (7), with feldspar and quartz products of the same reaction:

$$\mathrm{Bt} + \mathrm{Ky} + \mathrm{Qtz} \leftrightarrow \mathrm{Grt} + \mathrm{Kfs} + \mathrm{M}. \quad (7)$$

Textures related to retrometamorphism are common, as it was an intense process in all rocks of the Serra da Natureza Klippe. Kyanite is partially replaced by skeletal intergrowths of biotite and sillimanite (Fig. 4e) due to the crossing of reaction (7) from high to low temperature in minimum conditions of 850 °C and 10 kbar. In addition, in some samples, a groundmass of fine-grained muscovite occurs around kyanite (Fig. 4c), even forming pseudomorphs.

It is considered that the rocks of Serra da Natureza Klippe achieved the metamorphic peak at high-pressure granulite facies, progressing from the staurolite stability field, crossing muscovite and biotite melting reactions within the kyanite field at 815–850 °C and 16 kbar, which was followed by decompression, and cooling when the rocks crossed re-hydration reactions within the sillimanite field.

A metamorphic map is drawn with the distinct mineral assemblages from all units (Fig. 2). In the Andrelândia Nappe domain, the staurolite-out isograd is drawn parallel to the tectonic contact with the Liberdade Nappe, with the presence of staurolite at the top of the structure and its absence at the base. In the Liberdade Nappe domain, the staurolite-out and melt-in isograds are coincident due to a small overlap between the highest temperature portion of the staurolite field with the melting-in reactions involving a reaction that uses muscovite and albite as reactants for the first generation of melt in very low quantities, as discussed previously (Spear et al. 1999), until its widespread recognition. Within the stack of the Serra da Natureza Klippe rocks, no isograd is recognized and all of them present the same high-pressure granulite facies mineral assemblage. The isograd disposition indicates an inverted metamorphic pattern inside the Andrelândia Nappe domain and a normal metamorphic pattern inside the Liberdade Nappe domain. An apparent metamorphic inversion occurs due to the overthrusting of high-pressure granulites of the Serra da Natureza Klippe over amphibolite facies rocks of the Liberdade Nappe. Thus, a true metamorphic inversion is only observed inside the Andrelândia Nappe.

Mineral chemistry

The chemical compositions of minerals were analyzed in the Institute of Geosciences, São Paulo University, using a JEOL Electron Microprobe, model JXA-8600, under conditions of 15 kV and 20 nA, with a beam diameter ranging between 5 and 15 μm and natural minerals used as standards for all elements. For rutile analyses, the protocol established by Zack et al. (2004) was followed. Seven samples were analyzed (Tables 1, 2, 3, 4): two from Andrelândia Nappe, one from Santo Antônio schist from the base of the structure with staurolite (SN27), and one from Serra da Boa Vista schist at the top of structure without staurolite (SN160); three samples from the Liberdade Nappe, with a metatexite at its base (SN161); another from the intermediate portion of the structure (SN128); and a staurolite–kyanite–biotite–garnet schist at its top (SN64); two samples from the Serra da Natureza Klippe were analyzed, both rutile–kyanite–garnet–orthoclase granulite (SN52 and 96).

Garnet was analyzed in all samples. Overall, cores of garnet grains are enriched in pyrope, grossular, and spessartite, decreasing towards the rim, whereas almandine has lower concentrations in the core and increases gradually towards the rim (Fig. 5; Table 1). In all units, almandine is the highest end member and spessartite is the lowest. Pyrope is commonly higher than grossular; in garnet cores in the Andrelândia Nappe, the grossular content is higher than that of pyrope. In the Liberdade Nappe and Serra da Natureza Klippe, the end members exhibit flat behavior.

Biotite occurs in all samples, and analyses were normalized to 11 oxygen atoms. In both samples of the Andrelândia Nappe, biotite XMg is 0.55 and the Ti contents are 0.1 apfu. Biotite in samples of the basal portion of the Liberdade Nappe has a similar XMg, between 0.47 and 0.49, but the Ti contents are predominantly lower, between 0.088 and 0.138 apfu. At the top of the Liberdade Nappe, XMg is similar to that in the other samples in the matrix grains (0.47), but the inclusions in garnet exhibit a higher XMg of ~0.56, whereas the Ti contents are lower than in the other samples (0.077–0.106 apfu), with no distinction between its textural context. In the Serra da Natureza Klippe, grains have higher Ti contents than in the other units (between 0.210 and 0.236 apfu), and XMg is 0.42 in matrix grains and 0.49 in garnet inclusions (Table 2).

Muscovite analyses were also normalized to 11 oxygen atoms. Muscovite takes part in the peak metamorphic paragenesis of samples of the Andrelândia and Liberdade Nappes and is only present in the retrograde phase in the Serra da Natureza Klippe samples, where it was not analyzed. The Mg content in the samples of Liberdade Nappe (SN161, 128 and 64) are between 0.06 and 0.08 apfu and are lower than those of the Andrelândia Nappe (SN27, 160), that is, between 0.05 and 0.1 apfu (Table 3).

Staurolite only occurs in samples of the Andrelândia Nappe base (SN27) and at the Liberdade Nappe top (SN64). In the Andrelândia Nappe, the XMg values range from 0.21, at the grain cores, to 0.18, at the rims, and Ti ranges from 0.16 to 0.08 apfu. In the Liberdade Nappe, there is no variation in staurolite composition from core to rim, with an average XMg of 0.15, and Ti of 0.12 apfu (Table 3).

Plagioclase occurs in samples of the Andrelândia Nappe and in two samples of the basal portion of the Liberdade Nappe. In the Santo Antônio schist (SN27) of the Andrelândia Nappe, the plagioclase composition is An30, and in the Serra da Boa Vista schist (SN160), it is An22. At the base of the Liberdade Nappe (SN161), the plagioclase composition is An29, whereas for the intermediate portion sample (SN128), it is An25 (Table 4).

Orthoclase is only present in samples of the Serra da Natureza Klippe (SN52 and 96), with an average composition of Or86 and an exsolution composition of An25 (Table 4).

Rutile was analyzed in all samples. The highest concentration of Zr, Nb, and V occurs in the samples containing leucosome, that is, samples from the Serra da Natureza Klippe and those from the base and intermediate portions of the Liberdade Nappe (Table 5).

Thermobarometry

Pressure and temperature determinations were performed on samples of all three units using Zr as a rutile thermometer (Fig. 6), experimentally calibrated by Tomkins et al. (2007), and the program THERMOCALC, v.3.32, using the average *P–T* mode (Powell and Holland 1994). All of the results are summarized in Table 6.

The *P–T* conditions calculated with THERMOCALC for the Andrelândia Nappe base, with staurolite-bearing paragenesis, are 668 ± 15 °C and 9.1 ± 0.7 kbar (Fig. 7a), whereas the Zr provides an average of 610 °C and a maximum of approximately 622 °C. For the top of the Andrelândia Nappe, using paragenesis without staurolite, THERMOCALC calculates 665 ± 17 °C and 10.45 ± 0.74 kbar (Fig. 7a) and Zr yields a value of 649 °C, on average, with a maximum temperature of 686 °C. Because the stack of the Andrelândia Nappe is not thick in the study area, the differences in the calculated *P–T* conditions are not significant; even if it has been determined as an inverted metamorphic pattern from the observed paragenesis, the rutile thermometry records a higher temperature variation.

For the Liberdade Nappe samples, the results obtained with THERMOCALC for the base, intermediate,

Table 1 Selected analyses of garnet

Sample	SN27	SN27	SN160	SN160	SN160	SN161	SN161	SN128	SN128	SN64	SN64	SN52	SN52	SN52	SN96	SN96
Location	ANB	ANB	ANT	ANT	ANT	LNB	LNB	LNI	LNI	LNB	LNB	SNK	SNK	SNK	SNK	SNK
Position	Core	Rim	Core	Inter	Rim	Core	Rim	Core	Rim	Core	Rim	Core	Inter	Rim	Core	Rim
SiO_2	37.24	37.76	37.23	37.91	37.59	37.77	37.94	37.52	37.55	37.33	36.73	37.9	37.45	38.05	37.47	37.24
TiO_2	0	0.04	0.01	0.01	0	0.01	0	0	0	0.1	0	0	0	0	0	0.01
Al_2O_3	21.6	22.03	21.52	21.66	21.93	21.92	22.18	21.92	21.79	21.59	21.66	21.86	21.86	22.2	21.98	21.94
Cr_2O_3	0	0	0	0	0	0	0	0	0	0	0	0	0	0	0	0
Fe_2O_3	1.18	0.91	0	0	0	0	0	0	0	0	0.71	0.28	0	0	0.83	0
FeO	30.59	30.95	27.42	32.53	32.88	35.77	34.49	35.51	35.99	35.63	36.78	33.92	35.39	34.03	35.97	36.6
MnO	4.13	0.69	3.62	1.9	1.11	0.97	0.79	1.06	1.11	0.74	0.8	1.6	0	0	0.68	0.77
MgO	3.54	4.15	0.7	2.46	3.36	3.1	4.02	3.18	2.82	3.66	3.13	3	4.48	4.28	4.16	3.21
CaO	2.67	4.79	9.14	3.78	3.57	1.99	1.65	2.04	1.9	1.27	0.59	3.46	0	2.77	0.57	0.95
Na_2O	0	0	0	0	0	0	0	0	0	0	0	0	0	0	0	0
K_2O	0	0	0	0	0	0	0	0	0	0	0	0	0	0	0	0
Total	100.85	101.23	99.63	100.25	100.45	101.54	101.06	101.24	101.17	100.32	100.32	102	99.19	101.34	101.67	100.71
Oxygens	12	12	12	12	12	12	12	12	12	12	12	12	12	12	12	12
Si	2.954	2.955	2.991	3.019	2.982	2.985	2.988	2.975	2.986	2.982	2.952	2.979	2.999	2.981	2.954	2.972
Ti	0	0.002	0.001	0	0	0.001	0	0	0	0.006	0	0	0	0	0	0.001
Al	2.021	2.033	2.039	2.034	2.052	2.043	2.059	2.049	2.043	2.033	2.052	2.026	2.064	2.051	2.043	2.064
Cr	0	0	0	0	0	0	0	0	0	0	0	0	0	0	0	0
Fe^{3+}	0.07	0.053	0	0	0	0	0	0	0	0	0.043	0.017	0	0	0.049	0
Fe^{2+}	2.03	2.026	1.842	2.167	2.182	2.365	2.272	2.355	2.394	2.381	2.473	2.23	2.371	2.23	2.372	2.443
Mn	0.278	0.045	0.246	0.128	0.074	0.065	0.053	0.071	0.075	0.05	0.054	0.106	0	0	0.045	0.052
Mg	0.419	0.484	0.083	0.292	0.397	0.365	0.472	0.376	0.334	0.435	0.374	0.352	0.534	0.5	0.489	0.382
Ca	0.227	0.402	0.788	0.323	0.304	0.169	0.139	0.173	0.162	0.109	0.051	0.291	0	0.232	0.048	0.081
Na	0	0	0	0	0	0	0	0	0	0	0	0	0	0	0	0
K	0	0	0	0	0	0	0	0	0	0	0	0	0	0	0	0
Sum	8	8	7.989	7.963	7.992	7.993	7.982	8	7.993	7.996	8	8	7.969	7.994	8	7.995
alm	68.7	68.5	62.3	74.5	73.8	79.8	77.4	79.2	80.7	80.0	83.8	74.9	81.6	75.3	80.3	82.6
prp	14.2	16.4	2.8	10.0	13.4	12.3	16.1	12.6	11.3	14.6	12.7	11.8	18.4	16.9	16.6	12.9
sp	9.4	1.5	8.3	4.4	2.5	2.2	1.8	2.4	2.5	1.7	1.8	3.6	0.0	0.0	1.5	1.8
grs	4.3	11.1	26.6	11.1	10.3	5.7	4.7	5.8	5.5	3.7	0.0	8.9	0.0	7.8	0.0	2.7

ANB Andrelândia Nappe base, *ANT* Andrelândia Nappe top, *LNB* Liberdade Nappe base, *LNI* Liberdade Nappe intermediate, *LNT* Liberdade Nappe top, *SNK* Serra da Natureza Klippe, *alm* almandine, *prp* pirope, *sp* spessartite, *grs* grossular, *inter* between core and rim

Table 2 Selected analyses of biotite

Sample	SN27	SN27	SN160	SN160	SN161	SN161	SN128	SN128	SN64	SN64	SN52	SN52	SN96	SN96
Location	ANB	ANB	ANT	ANT	LNB	LNB	LNI	LNI	LNT	LNT	SNK	SNK	SNK	SNK
SiO_2	36.31	36.38	35.93	36.13	35.12	35.25	35.5	35.78	36.23	35.49	36.05	35.98	35.64	35.52
TiO_2	1.59	1.7	1.89	1.48	2.17	1.76	2.06	2.17	1.64	1.66	2.78	2.92	3.83	3.76
Al_2O_3	19.05	18.87	19.2	19.75	19.18	19.67	18.83	19.5	19.53	19.12	18.7	19.14	18.8	18.59
Cr_2O_3	0	0	0	0	0	0	0	0	0	0	0	0	0	0
Fe_2O_3	0	0	0	0	0	0	0	0	0	0	0	0	0	0
FeO	16.57	16.76	17.27	17.27	19.06	18.97	18.36	19.07	16.01	19.8	17.84	18.01	18.07	17.36
MnO	0.09	0.1	0.01	0.04	0	0.05	0.04	0.02	0.02	0.03	0	0.03	0.01	0
MgO	11.98	11.96	11.29	11.32	10.05	9.92	10.23	10.08	12.2	9.76	9.82	9.78	9.42	9.5
CaO	0	0	0	0	0	0.03	0	0	0	0	0	0	0.03	0.02
Na_2O	0.23	0.31	0.21	0.15	0.23	0.28	0.29	0.28	0.36	0.22	0.12	0.16	0.15	0.14
K_2O	9.18	8.99	9.35	9.36	9.01	8.99	9.19	9.23	8.95	8.89	9.88	9.71	9.97	9.53
Total	95.02	95.08	95.18	95.5	94.83	94.93	94.52	96.14	94.95	94.98	95.2	95.73	95.94	94.41
Oxygens	11	11	11	11	11	11	11	11	11	11	11	11	11	11
Si	2.725	2.729	2.705	2.706	2.677	2.68	2.708	2.687	2.709	2.705	2.729	2.707	2.685	2.704
Ti	0.09	0.096	0.107	0.083	0.124	0.1	0.118	0.123	0.092	0.095	0.158	0.165	0.217	0.215
Al	1.685	1.669	1.704	1.744	1.724	1.763	1.693	1.726	1.721	1.718	1.669	1.698	1.67	1.669
Cr	0	0	0	0	0	0	0	0	0	0	0	0	0	0
Fe^{3+}	0	0	0	0	0	0	0	0	0	0	0	0	0	0
Fe^{2+}	1.04	1.052	1.087	1.082	1.215	1.206	1.172	1.198	1.001	1.262	1.129	1.133	1.139	1.105
Mn	0.006	0.006	0.001	0.002	0	0.003	0.003	0.001	0.001	0.002	0	0.002	0.001	0
Mg	1.34	1.337	1.267	1.263	1.142	1.125	1.163	1.128	1.36	1.109	1.108	1.097	1.057	1.078
Ca	0	0	0	0	0	0.002	0	0	0	0	0	0	0.002	0.001
Na	0.033	0.045	0.031	0.022	0.033	0.042	0.044	0.041	0.052	0.032	0.018	0.023	0.022	0.02
K	0.879	0.86	0.899	0.896	0.877	0.873	0.895	0.885	0.854	0.865	0.954	0.932	0.959	0.927
Sum	7.799	7.794	7.801	7.798	7.792	7.796	7.796	7.790	7.792	7.790	7.765	7.757	7.753	7.720

ANB Andrelândia Nappe base, *ANT* Andrelândia Nappe top, *LNB* Liberdade Nappe base, *LNI* Liberdade Nappe intermediate, *LNT* Liberdade Nappe top, *SNK* Serra da Natureza Klippe

and top portions are, respectively, 714 ± 29 °C and 10.22 ± 1.03 kbar, 678 ± 60 °C and 8.4 ± 1.39 kbar, and 642 ± 28 °C and 7.53 ± 2.95 kbar (Fig. 7b). The data obtained with the Zr show averages of 711, 714 and 692 °C for the base, intermediate, and top portions, respectively. The maximum temperatures calculated from Zr-in-rutile are 754, 740, and 743 °C, respectively. The results show a strong gradient of decreasing temperatures towards the top of the structure, implying a normal pattern for metamorphism. The results of pressure are consistent with the thickness of the stack.

The *P–T* conditions calculated with THERMOCALC for the Serra da Natureza Klippe samples are 815 ± 47 °C and 16.6 ± 5.8 kbar, and 801 ± 49 °C and 13.7 ± 6.4 kbar (Fig. 7c). The Zr yielded considerably lower temperatures, averaging between 764 and 758 °C, with a maximum between 782 and 790 °C, which are probably related with retrometamorphism; because most rutile grains are associated with ilmenite and sometimes zircon grains (Fig. 4f). The texture is mainly related to the destabilization of rutile, which loses Zr to form zircon via reaction (8). Even if most of the analyzed grains are inclusions in garnet, with no apparent retrometamorphic texture, low calculated temperatures might result from analyses of grains trapped before the metamorphic peak:

$$\mathrm{Zr(in\ Rt)} + \mathrm{Grt} \leftrightarrow \mathrm{Zrc} + \mathrm{Ilm}. \quad (8)$$

Integrating information from mineral assemblages, reaction textures, and thermobarometry, three parallel *P–T* paths were inferred for each of the three allochthons (Fig. 7a–c). They are all portions of clockwise *P–T* paths, whose rocks achieved their peak in the kyanite stability field, presenting different retrogression paths, but all crossed the sillimanite field after reaching their metamorphic peak.

Table 3 Selected analyses of muscovite and staurolite

Sample	SN27	SN27	SN160	SN160	SN161	SN161	SN128	SN128	SN64	SN64	SN27	SN27	SN64	SN64
Location	ANB	ANB	ANT	ANT	LNB	LNB	LNI	LNI	LNT	LNT	ANB	ANB	LNT	LNT
Mineral	Muscovite	Muscovite	Muscovite	Muscovite	Muscovite	Muscovite	Muscovite	Muscovite	Muscovite	Muscovite	Staurolite	Staurolite	Staurolite	Staurolite
SiO_2	46.19	45.65	46.74	45.65	45.78	45.51	45.79	46.38	46.34	47.31	27.21	27.4	27.18	28
TiO_2	0.59	0.39	0.91	1.05	1.43	1.99	0.64	0.57	0.59	0.72	0.61	0.62	0.54	0.68
Al_2O_3	34.88	35.23	34.17	35.13	35.14	35.12	35.94	35.72	35.32	35.19	52.94	53.06	54.04	53.14
Cr_2O_3	0	0	0	0	0	0	0	0	0.00	0.00	0.01	0.03	0.09	0.04
Fe_2O_3	0	0	0	0	0	0	0	0	0.00	0.00	0	0	0	0
FeO	2.29	2.19	1.13	1.07	1.46	1.09	1.15	1.07	1.22	1.08	14.49	14.3	14.46	14.52
MnO	0	0	0	0	0	0	0.01	0.03	0.00	0.00	0.26	0.27	0.03	0.03
MgO	0.72	0.65	1.07	0.79	0.76	0.66	0	0	0.60	0.76	2.06	2.09	1.45	1.55
CaO	0	0	0	0	0	0.02	0	0	0.00	0.00	0	0	0	0
Na_2O	1.39	1.48	0.85	0.97	0.87	0.88	0	0	0.88	0.77	0.01	0.02	0	0.01
K_2O	9.19	9.1	10.37	10.19	10.15	10.15	10.1	9.99	9.83	9.80	0	0	0	0
Total	95.24	94.68	95.25	94.87	95.61	95.42	93.64	93.76	94.79	95.64	97.61	97.79	97.79	97.96
Oxygens	11	11	11	11	11	11	11	11	11	11	46	46	46	46
Si	3.077	3.058	3.111	3.052	3.042	3.028	3.08	3.109	3.088	3.117	7.614	7.643	7.573	7.781
Ti	0.03	0.019	0.046	0.053	0.072	0.099	0.033	0.029	0.03	0.036	0.129	0.13	0.113	0.141
Al	2.739	2.782	2.681	2.769	2.753	2.754	2.85	2.823	2.775	2.733	17.462	17.447	17.748	17.412
Cr	0	0	0	0	0	0	0	0	0	0	0.003	0.007	0.02	0.01
Fe^{3+}	0	0	0	0	0	0	0	0	0	0	0	0	0	0
Fe^{2+}	0.127	0.123	0.063	0.06	0.081	0.06	0.065	0.06	0.068	0.059	3.39	3.336	3.368	3.374
Mn	0	0	0	0	0	0	0	0.002	0	0	0.062	0.063	0.006	0.007
Mg	0.071	0.065	0.106	0.078	0.076	0.065	0	0	0.059	0.075	0.861	0.868	0.603	0.641
Ca	0	0	0	0	0	0.001	0	0	0	0	0	0	0	0
Na	0.179	0.192	0.11	0.126	0.112	0.113	0	0	0.113	0.099	0.007	0.009	0	0.003
K	0.781	0.778	0.882	0.87	0.861	0.862	0.868	0.855	0.837	0.825	0	0	0	0
Sum	7.004	7.017	6.998	7.009	6.996	6.984	6.896	6.878	6.970	6.943	29.527	29.504	29.431	29.369

ANB Andrelândia Nappe base, *ANT* Andrelândia Nappe top, *LNB* Liberdade Nappe base, *LNI* Liberdade Nappe intermediate, *LNT* Liberdade Nappe top

Table 4 Selected analyses of feldspar

Sample	SN27	SN27	SN160	SN160	SN161	SN161	SN128	SN128	SN52	SN52	SN52	SN96	SN96
Location	ANB	ANB	ANT	ANT	LNB	LNB	LNI	LNI	SNK	SNK	SNK	SNK	SNK
Mineral	Plagioclase	Plagioclase	Plagioclase	Plagioclase	Plagioclase	Plagioclase	Plagioclase	Plagioclase	K-feldspar	Mesoperthite	Mesoperthite	K-feldspar	K-feldspar
Position	Core	Rim	Core	Rim	Core	Rim	Core	Rim	Residum	Host	Exsolution	Core	Rim
SiO_2	61.18	61.05	63.51	62.49	61.95	62.23	61.94	62.18	64.95	65.26	63.82	64.24	64.51
TiO_2	0	0	0	0	0.01	0.02	0	0	0.06	0	0	0.05	0.00
Al_2O_3	24.85	24.41	23.41	23.82	24.26	24.61	24.32	24.02	18.93	19.19	22.9	18.69	19.27
Cr_2O_3	0	0	0	0	0.00	0.00	0	0	0	0	0	0.00	0.00
Fe_2O_3	0	0	0.06	0.2	0.01	0.10	0.08	0.1	0	0.04	0.03	0.00	0.00
FeO	0	0	0	0	0.00	0.00	0	0	0	0	0	0.00	0.00
MnO	0.04	0	0.01	0	0.00	0.00	0.01	0.02	0.03	0	0	0.00	0.00
MgO	0	0	0	0	0.01	0.00	0	0.01	0.01	0.01	0.01	0.01	0.00
CaO	6.46	5.89	4.52	4.64	4.92	5.02	5.34	5.29	0.14	0.03	3.71	0.01	0.00
Na_2O	7.97	8.16	8.81	8.75	8.78	8.66	8.51	8.2	1.76	1.73	8.95	1.51	1.64
K_2O	0.05	0.05	0.09	0.09	0.07	0.09	0.05	0.07	14.25	14.21	0.61	14.61	14.26
Total	100.55	99.55	100.41	100	100.00	100.73	100.26	99.9	100.14	100.49	100.02	99.13	99.69
Oxygens	8	8	8	8	8.0	8.0	8	8	8	8.0	8.0	8.0	8.0
Si	2.704	2.718	2.793	2.764	2.743	2.736	2.738	2.753	2.978	2.978	2.817	2.981	2.969
Ti	0	0	0	0	0	0.001	0	0	0.002	0	0	0.002	0
Al	1.295	1.281	1.214	1.242	1.266	1.276	1.267	1.254	1.023	1.033	1.192	1.022	1.046
Cr	0	0	0	0	0	0	0	0	0	0	0	0	0
Fe^{3+}	0	0.006	0.002	0.007	0	0.003	0.003	0.003	0	0.001	0.001	0	0
Fe^{2+}	0	0	0	0	0	0	0	0	0	0	0	0	0
Mn	0.001	0	0	0	0	0	0	0.001	0.001	0	0	0	0
Mg	0	0	0	0	0	0	0	0.001	0	0.001	0	0.001	0
Ca	0.306	0.281	0.213	0.22	0.234	0.236	0.253	0.251	0.007	0.002	0.175	0	0
Na	0.683	0.705	0.751	0.75	0.754	0.738	0.729	0.704	0.157	0.153	0.766	0.136	0.146
K	0.003	0.003	0.005	0.005	0.004	0.005	0.003	0.004	0.834	0.828	0.034	0.866	0.838
Sum	4.992	4.992	4.978	4.989	5.002	4.995	4.993	4.972	5.003	4996	4986	5.008	5
or	0.30	0.30	0.52	0.51	0.40	0.51	0.30	0.42	83.57	84.23	3.49	86.43	85.16
ab	68.85	71.28	77.50	76.92	76.01	75.38	74.01	73.41	15.73	15.56	78.56	13.57	14.84
an	30.85	28.41	21.98	22.56	23.59	24.11	25.69	26.17	0.70	0.20	17.95	0.00	0.00

ANB Andrelândia Nappe base, *ANT* Andrelândia Nappe top, *LNB* Liberdade Nappe base, *LNI* Liberdade Nappe intermediate, *SNK* Serra da Natureza Klippe, *or* orthoclase, *ab* albite, *an* anorthite

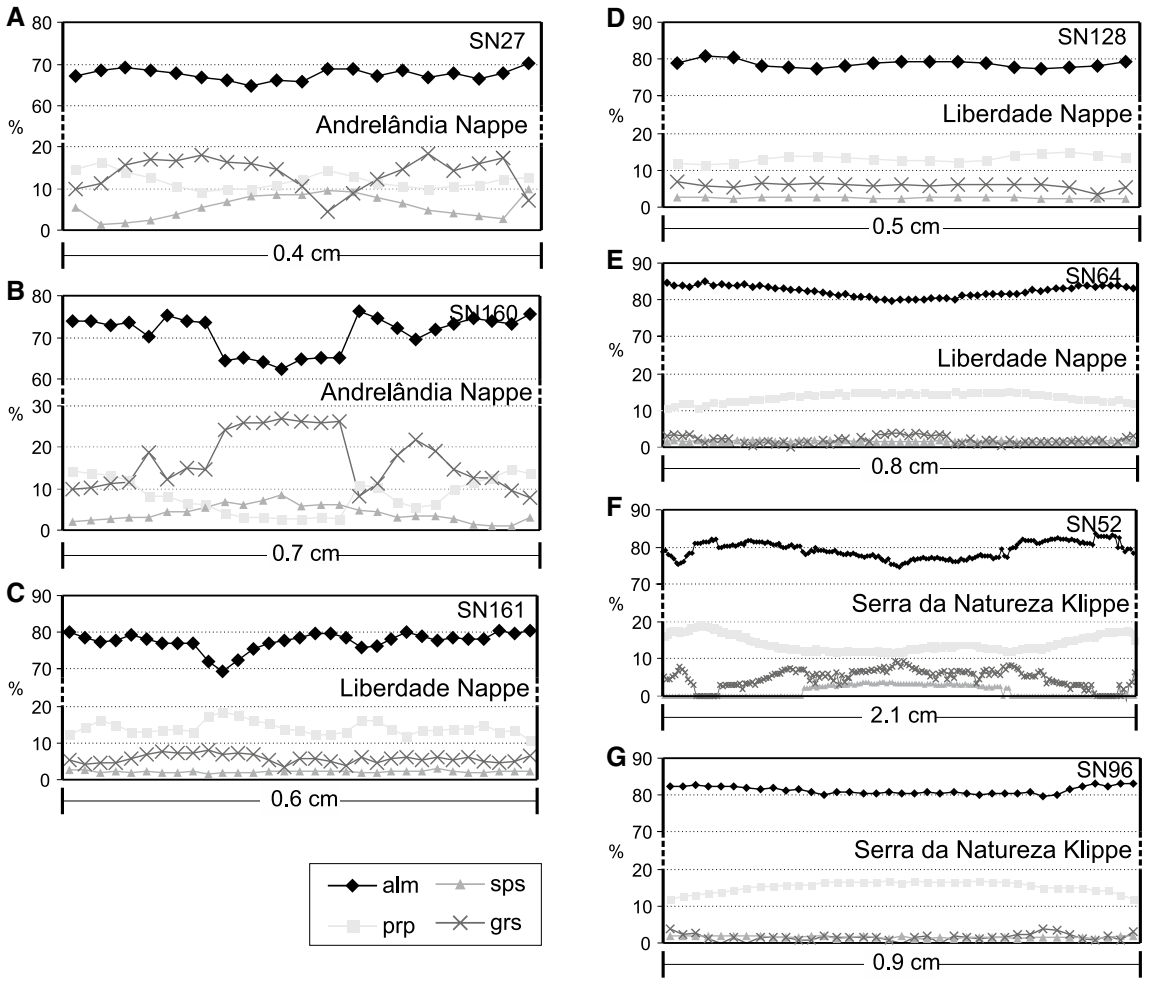

Fig. 5 Changes in almandine, pyrope, spessartine, and grossular components along garnet porphyroblasts. **a** Andrelândia Nappe bottom; in this grain, the almandine and grossular increase from the core to rim, whereas spessartine and pyrope decrease; the last two points show a retrograde rim with increasing spessartine and decreasing of the other members. **b** Andrelândia Nappe top; spessartite exhibits a flat pattern with a slight decrease. Pyrope and almandine display opposite behavior to grossular, which has high grades in the core, low shoulders with slight increases in the intermediate part, and a negative slope toward to the rim; **c** Liberdade Nappe bottom; spessartine and grossular exhibit a flat pattern, almandine slightly increases toward the rim, and pyrope slightly decreases; **d** Liberdade Nappe intermediate portion; the grain has a flat distribution of its end members; **e** Liberdade Nappe top; the garnet shows a flat distribution; **f** Serra da Natureza Klippe; the garnet exhibits enrichment of almandine and pyrope, which decrease towards the rim, and spessartine occurs only in the core. There is a fine retrograde rim where grossular increases and almandine and pyrope decrease. **g** Serra da Natureza; the grain has a flat pattern of distribution of end members with a slight decrease of pyrope toward the rim

Monazite dating

Monazite can be used as a chemical dating method. In this study, quantitative determinations of elements were performed in the Institute of Geosciences, São Paulo University, using a JEOL JXA-8600S electron microprobe, with a 15 kV accelerating voltage, a current of 300 nA, and a beam diameter of 2–4 μm. In Brazil, the technique was developed by Vlach and Gualda (2000) and improved by Martins et al. (2009), and their standardization protocol is followed here. Two in-house natural monazite standards (Em-013A and S3-167; Vlach 2010) were used for EPMA U–Th–Pb_T dating calibration and the standard data are reported in Table S1 (Supplementary material). The data were collected in a single analytical session and the standard was analyzed before and after the session. Table 7 presents the measurement results and the associated uncertainties in 2σ for U, Th, and Pb. In each spot, data were calculated following the procedures of Vlach (2010). The mean ages (at 95% confidence level) were calculated using the weighted average tool of Isoplot 3.0 (Ludwig 2003), considering only the internal errors.

In rocks of the Andrelândia Nappe, monazite is scarce, and only one grain was recognized in the matrix of the

Table 5 Analyses of rutile showing the highest Zr amount in each sample

Sample	SN27	SN160	SN161	SN128	SN64	SN52	SN96
Location	ANB	ANT	LNB	LNI	LNT	SNK	SNK
TiO_2	98.57	99.12	100.75	92.59	97.99	92.27	92.67
SiO_2	0.04	0.03	0.01	0.05	0.02	0.01	0.01
Cr_2O_3	0.15	0.17	0.04	0.04	0.05	0.09	0.12
Al_2O_3	0.13	0.14	0.13	0.17	0.16	0.12	0.14
Nb_2O_5	0.37	0.87	0.32	0.42	0.45	0.45	1.17
FeO	0.56	0.48	0.62	1.11	0.56	0.17	0.81
V_2O_5	0.41	0.48	0.35	0.39	0.44	0.52	0.59
ZrO_2	0.03	0.06	0.13	0.12	0.10	0.14	0.14
SnO_2	0.01	0.01	0.03	0.03	0.01	0.02	0.02
Total	100.253	101.359	102.369	94.91	99.784	93.777	95.648
Oxygens	2	2	2	2	2	2	2
Ti	0.98646	0.98387	0.98598	0.97699	0.98544	0.98900	0.97543
Si	0.00028	0.00022	0.00008	0.00041	0.00013	0.00010	0.00008
Cr	0.00083	0.00097	0.00020	0.00022	0.00028	0.00050	0.00069
Al	0.00056	0.00061	0.00056	0.00078	0.00073	0.00060	0.00063
Nb	0.00215	0.00504	0.00183	0.00260	0.00265	0.00280	0.00716
Fe	0.00728	0.00613	0.00784	0.01515	0.00725	0.00240	0.01103
V	0.00191	0.00224	0.00159	0.00193	0.00206	0.00260	0.00288
Zr	0.00037	0.00075	0.00156	0.00150	0.00128	0.00179	0.00177
Sn	0.00016	0.00017	0.00036	0.00042	0.00019	0.00030	0.00033

ANB Andrelândia Nappe base, *ANT* Andrelândia Nappe top, *LNB* Liberdade Nappe base, *LNI* Liberdade Nappe intermediate, *LNT* Liberdade Nappe top, *SNK* Serra da Natureza Klippe

Santo Antônio schist, which is xenoblastic and associated with the minerals that define the main foliation, S_2, and was developed during the metamorphic peak. The grain has just one compositional domain and the dates resulted from each analyzed point are homogeneous, with an average of 586 ± 15 Ma (Fig. 8a).

At the top of the Liberdade Nappe, in the staurolite-garnet schist, five monazite grains were analyzed. Grains in the matrix and in garnet were chosen for the analysis. Both types of grains are xenoblastic, with elongated zones that present different chemical compositions, which, however, do not yield different dates. The average age of all textures and grains is 622.3 ± 7.6 Ma (Fig. 8b).

Seven monazite grains from one sample of the Serra da Natureza Klippe were analyzed. All were xenoblastic and occurred in the matrix, wider than 10 μm, or as inclusions in garnet, smaller than 10 μm. both domains yield an average age of 604.5 ± 6.1 Ma (Fig. 8c).

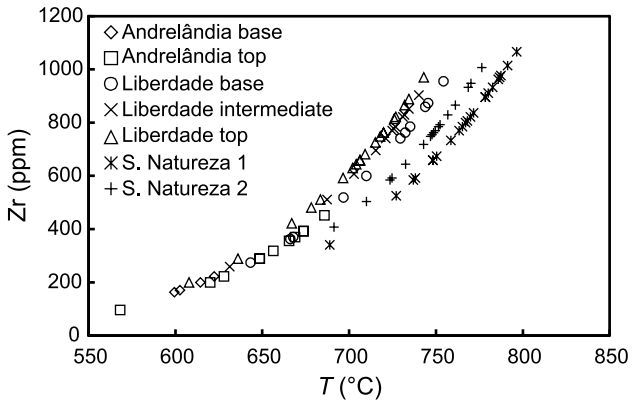

Fig. 6 Diagram of temperature versus Zr content in rutile based on the Tomkins et al. (2007) thermometer, which was calculated with pressures obtained by THERMOCALC (Table 6)

Models and discussion

The topmost unit, the Serra da Natureza Klippe, is characterized by high-pressure granulites with a mineral assemblage composed of rutile–kyanite–garnet–orthoclase–quartz, which attained a metamorphic peak above 800 °C and 13 kbar (Fig. 7; Table 6). Monazite ages suggest metamorphic peak at 604.5 ± 6.1 Ma by isothermal relaxation. This age is a little younger than the data obtained from rocks in related units, that is, the Três Pontas-Varginha Nappe and the Carvalhos Klippe (Campos Neto et al. 2010; Reno et al. 2012; Trouw et al. 2008). Although a strong geological correlation is found between the Serra da Natureza Klippe and the Três Pontas-Varginha Nappe, the former may represent a slightly colder crustal fragment, as

Table 6 Thermobarometry results

	Andrelândia Nappe		Liberdade Nappe			Serra da Natureza Klippe	
Sample	SN27	SN160	SN161	SN128	SN64	SN52	SN96
Position	Base	Top	Base	Intermediate	Top		
THERMOCALC (Powell and Holland 1994)							
T (°C)	668 ± 15	665 ± 17	714 ± 29	678 ± 60	642 ± 28	815 ± 47	801 ± 49
P(kbar)	9.1 ± 0.7	10.45 ± 0.74	10.22 ± 1.03	8.4 ± 1.39	7.53 ± 2.95	16.64 ± 5.8	13.7 ± 6.4
Zr-in-Rt (Tomkins et al. 2007)							
T (°C)	622	686	754	740	743	782	790

Zr-in-rutile thermometry is performed with pressures obtained by THERMOCALC, and they are the highest results of many analyses

the metamorphic peak *P–T* conditions are slightly lower. For example, the conditions calculated for rocks of the Carvalhos Klippe are 850 °C at 15 kbar (Campos Neto et al. 2010; Cioffi et al. 2012; Motta et al. 2010; Reno et al. 2012), whereas those for the Três Pontas-Varginha Nappe are calculated as 840–880 °C and 15–13 kbar (Garcia and Campos Neto 2003; Martinez 2015). Alternatively, the metamorphic peak conditions for rocks of the Serra da Natureza Klippe might be underestimated, because retrometamorphism textures are very common. These include replacement of rutile by ilmenite + zircon, replacement of kyanite by muscovite, and rims of myrmekite surrounding K-feldspar, which implies that some minerals have changed composition in a partially open system, after the metamorphic peak.

The intermediate unit, the Liberdade Nappe, has a staurolite–kyanite-bearing paragenesis at its top, which reached a metamorphic peak at 642 ± 28 °C and 7.5 ± 2.9 kbar (Fig. 7; Table 6). The structure base has a staurolite-free paragenesis, with kyanite and leucosome present. For this portion, the metamorphic peak was attained at 714 ± 29 °C and 10.2 ± 1 kbar (Fig. 7; Table 6). For the intermediate portion of the structure, staurolite-free and kyanite and leucosome-bearing paragenesis can be identified, and the calculated *P–T* conditions are 678 ± 60 °C and 8.4 ± 1.4 kbar (Fig. 7; Table 6). This metamorphic set indicates a normal metamorphism pattern within the unit. The thickness of the pack, recognized during fieldwork, does not support such a pressure variation, which could be caused by unidentified secondary thrusts, although it still forms a coherent pack of rocks. The age of metamorphism is 622.3 ± 7.6 Ma, as determined by the monazite chemical dating using an electron microprobe.

The Andrelândia Nappe, that is, the lower unit, exhibits staurolite-bearing kyanite-free paragenesis that changes upward to staurolite–kyanite-bearing paragenesis. However, thermobarometric calculations do not support significant differences, 668 ± 15 °C at 9.1 ± 0.7 kbar, for kyanite-free paragenesis, and 665 ± 17 °C at 10.4 ± 0.7 kbar, for kyanite-bearing paragenesis (Fig. 7; Table 6). Nevertheless, the paragenesis and data of the previous works (Westin 2008) suggest an inverted metamorphic pattern within the unit. The monazite chemical age records the metamorphic peak at 586 ± 15 Ma.

Thus, in the study area, there are three allochthonous units, the Andrelândia Nappe, the Liberdade Nappe, and the Serra da Natureza Klippe, which present an inverted metamorphic pattern as a whole, but in detail, they frame a more complex picture. A true inverted pattern is only recognized within the Andrelândia Nappe, but both units at its top exhibit an increase in *P–T* conditions from top to bottom, demonstrating a normal metamorphic pattern. This pseudo-inverted metamorphism occurs by thrust faults, which were still active after the metamorphic peak.

Evolution of the Andrelândia Nappe System initiated with the collision between the San Franciscan and Paranapamena Plates. The Andrelândia basin was shortened and involved in the crustal thickening, disturbing the isotherms, and by 622 Ma, the Liberdade Nappe reached its metamorphic peak and experienced partial melting (Fig. 9a). After the crustal thickening and thermal relaxation combined with denudation of the upper crust, rocks of the Três Pontas-Varginha Nappe reached their metamorphic peak in 604 Ma (Fig. 9b). This process generated a hot surface with ductile rheology, which led to ascending flow of rocks, similar to channel flow extrusion. At this point, rocks from the margin of the São Francisco Craton were involved in the subduction process and progressively transported to the lower crust as a strong indenter into the orogen. The arrival of this colder and resistant block changed the tectonic style of the Neoproterozoic orogeny, and the leading edge of the indenter acted as a lower crustal ramp, upon which the Andrelândia Nappe System could be transported up, and exhumed by the combination of underthrusting and surface erosion. Rocks of the Liberdade Nappe, which were still hot, overthrusted those of the Andrelândia Nappe, folding the isotherms and hence inducing the inverted metamorphic pattern in the Andrelândia Nappe at 586 Ma

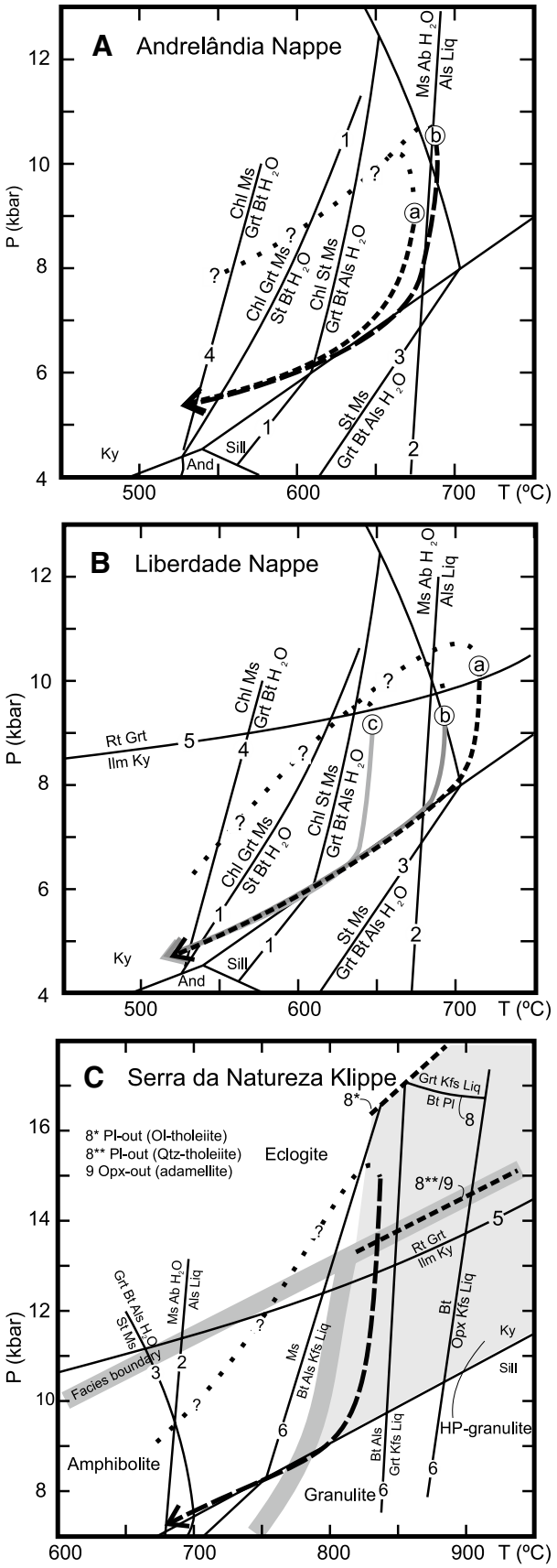

Fig. 7 *P–T* paths for the three allocations of the Andrelândia Nappe System, which show parallelism. **a** Andrelândia Nappe; *path a* is from the nappe base and *path b* is from the *top*; **b** Liberdade Nappe; *path a–c* are from the base to the *top*; **c** Serra da Natureza Klippe: *1* Powell et al. (1998); *2* Spear et al. (1999); *3* Spear and Cheney (1989); *4* Powell and Holland (1990); *5* Bohlen et al. (1983); *6* Vielzeuf and Holloway (1988); *7* Vielzeuf and Montel (1994); *8* Green and Ringwood (1967); and *9* Green and Lambert (1965)

(Fig. 9d). There are many exposures of the basement rocks within the Andrelândia Nappe System, and they are correlated chronologically and spatially with the São Francisco Craton (Cioffi et al. 2016). When the Três Pontas-Varginha Nappe and the indenter reached each other, some fragments were detached due to extreme stretching, which generated several klippen, such as the Serra da Natureza Klippe. This exhumation process fits the numerical model developed for the western portion of the Grenville Orogen (Jamieson et al. 2007, 2010), as well as the emplacement of this rigid block into the lower crust in the generation of the klippen and the isotherm folding.

If the *P–T* paths of the two uppermost allochthons are examined as a whole; in addition to their respective metamorphic peak conditions, the defined metamorphic field gradient is not typically barrovian (Fig. 10), as it plots between a series of high *P*/*T* and moderate *P*/*T* conditions compared to the rocks of the Greater Himalayas (Fraser et al. 2000; Vannay and Hodges 1996). The Andrelândia Nappe System defines a metamorphic field gradient with a shape similar to ocean–continent subduction zones (Winter 2001), although with higher *P–T* conditions, this is typical of the portions of the subducted lower continental crust.

Conclusions

The study segment of the Andrelândia Nappe System presents three allochthons: the Andrelândia and Liberdade Nappes, as well as the Serra da Natureza Klippe, and each one presents related yet independent metamorphic and tectonic evolutions. The distribution of the mineral assemblages within the Andrelândia Nappe indicates a metamorphic inversion, with rocks that record the highest *P–T* conditions located at the top of the structure. In the western portion of the area, which represents the closest exposure of the structure base, the association of staurolite, biotite, kyanite, quartz, and muscovite is the metamorphic peak paragenesis. In the eastern portion, the association of biotite, garnet, kyanite, quartz, and muscovite, without staurolite, is the metamorphic peak, which disappears along the contact with the Liberdade Nappe. The metamorphic peak mineral paragenesis of the Liberdade Nappe top is staurolite-bearing, whereas at its base, neither staurolite nor orthoclase is recognized, although leucosome

Table 7 Analytical data and ages for monazite realized by the electron microprobe

Unit/sample	Location	Grain	Th (ppm)		U (ppm)		Pb (ppm)		Ma		Average (Ma)
			Measured	Error (2σ)	Measured	Error (2σ)	Measured	Error (2σ)	Age	Error (2σ)	
Andrelândia Nappe/ SN27	Matrix	1	27,710	616	6424	187	1306	76	594	32	586 ± 15
		1	27,020	600	13,551	315	1957	90	607	25	
		1	30,930	679	8320	216	1454	86	556	30	
		1	29,890	660	12,841	303	1890	89	583	25	
		1	31,950	698	10,880	264	1778	88	584	26	
		1	28,100	623	11,809	285	1792	89	595	27	
		1	32,660	715	11,462	274	1820	89	575	25	
Liberdade Nappe/SN64	In Grt	1	37,400	810	4883	160	1534	87	636	33	622.3 ± 7.6
		1	37,400	810	4883	160	1535	87	637	33	
		1	34,380	746	4925	160	1415	86	621	35	
		1	38,890	837	4938	161	1552	87	625	32	
		1	38,740	835	5179	171	1524	86	607	32	
		1	39,440	848	5272	173	1614	87	630	31	
	Matrix	2	29,880	660	10,401	256	1758	88	609	27	
		2	29,180	643	4948	159	1298	75	633	34	
		2	32,590	713	6143	184	1422	85	598	33	
	Matrix	3	71,620	1496	13,669	325	3350	106	637	17	
		3	39,580	850	5021	162	1560	87	617	32	
		3	34,460	748	4444	154	1296	75	587	31	
		3	32,010	699	6569	190	1546	86	639	33	
	Matrix	4	73,860	1541	8815	237	2856	99	616	18	
		4	59,750	1257	11,952	293	2812	99	629	19	
		4	55,370	1168	10,927	269	2606	96	633	20	
		4	25,230	568	5529	174	1116	74	572	35	
	Matrix	5	21,790	498	5515	173	1100	74	611	38	
		5	15,690	383	1248	114	558	71	626	76	
		5	32,050	699	3949	147	1272	85	626	39	

Table 7 (continued)

Unit/sample	Location	Grain	Th (ppm)		U (ppm)		Pb (ppm)		Ma		Average (Ma)
			Measured	Error (2σ)	Measured	Error (2σ)	Measured	Error (2σ)	Age	Error (2σ)	
Serra da Natureza Klippe/SN52	Matrix	1	24,790	555	3994	147	995	73	583	40	604.5 ± 6.1
		1	35,070	759	4757	158	1384	76	606	30	
		1	29,690	652	4363	152	1160	74	585	35	
		1	32,160	702	4857	159	1296	75	598	32	
		1	36,870	796	2009	120	1194	74	610	35	
		1	30,230	666	4937	159	1286	75	614	33	
		1	32,880	719	4480	154	1304	75	608	32	
		1	30,230	666	4697	156	1216	74	591	34	
	Matrix	3	32,770	717	4551	155	1302	75	606	32	
		3	31,980	698	4259	151	1273	75	614	33	
		3	28,950	639	3121	138	1008	73	572	39	
		3	38,270	826	1704	118	1178	74	596	35	
	Matrix	4	28,890	638	3241	139	1098	74	616	38	
		4	37,460	811	4303	152	1397	76	601	30	
		4	33,110	723	4238	151	1252	75	591	33	
		4	35,140	760	4287	152	1381	76	622	31	
		4	47,850	1016	5355	175	1847	89	626	27	
		4	39,220	843	3724	146	1365	75	589	30	
	Matrix	5	36,170	783	3336	141	1243	75	586	33	
		5	38,900	837	3938	148	1368	86	586	34	
	Matrix	7	27,210	603	4279	151	1079	73	581	37	
		7	46,090	983	4943	162	1700	87	606	28	
		7	35,660	774	4601	156	1449	77	632	30	
	In Grt	2	26,900	602	3122	138	1045	73	624	41	
		2	30,240	666	3327	140	1105	74	596	37	
	In Grt	6	52,520	1110	1627	118	1595	87	612	30	
		6	59,020	1243	2379	134	1886	90	626	26	

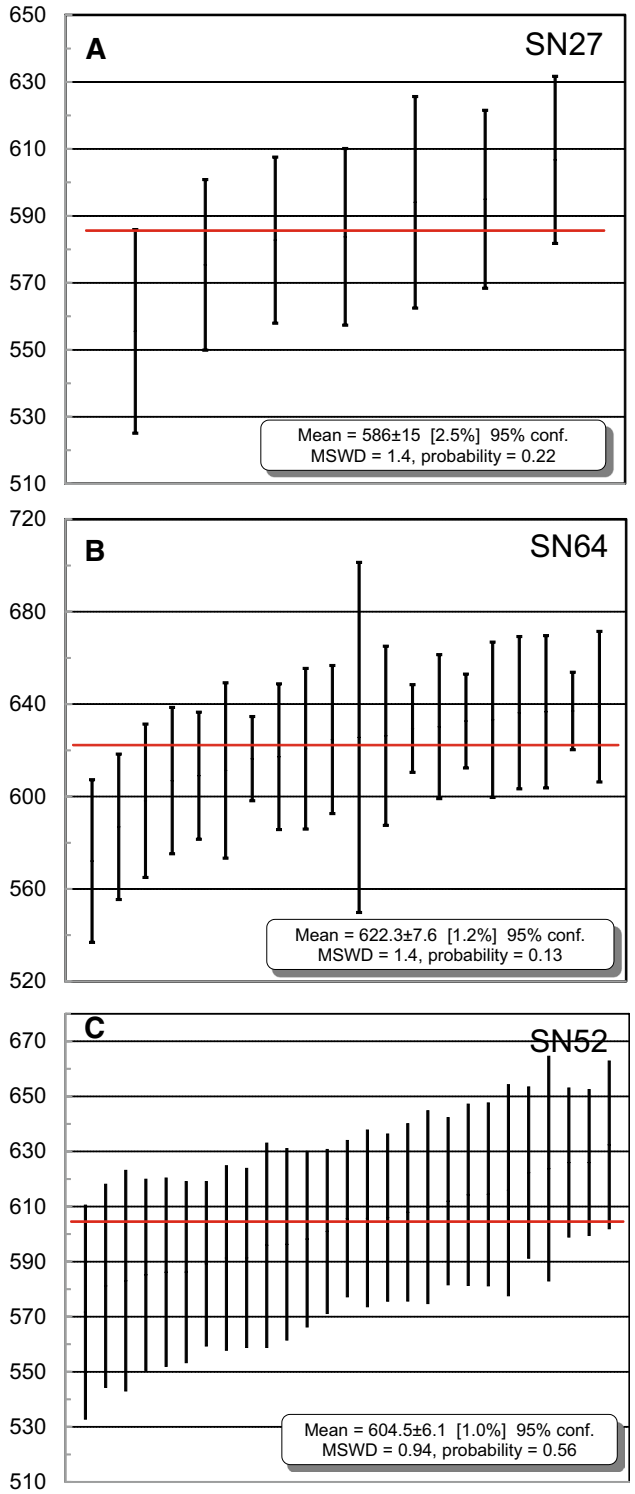

Fig. 8 Variation of ages and their uncertainties obtained using an electron microprobe: **a** Andrelândia Nappe; **b** Liberdade Nappe; **c** Serra da Natureza Klippe. *Vertical bars* represent the specific ages with 2σ associated uncertainty. *Horizontal bars* represent the average ages obtained for the appropriate population, which were defined by compositional domains in the monazite grains. The instrumental conditions were 15 kV, 300 nA, and 2–4 μm for the accelerating voltage

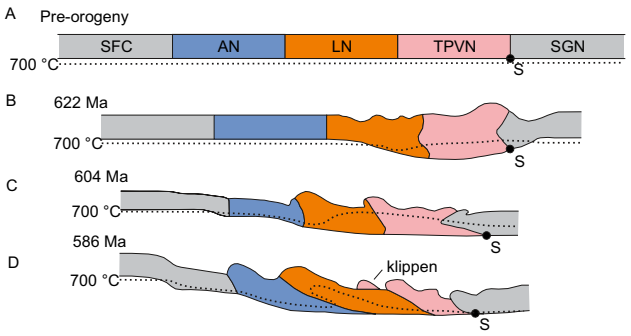

Fig. 9 Model for isotherms and tectonic evolution of the Andrelândia Nappe System. **a** Pre-orogenic state of units with bilateral relations; **b** age of the metamorphic peak of the Liberdade Nappe in 622 Ma; **c** isotherm relaxation and metamorphic peak of the Serra da Natureza Klippe in 604 Ma; **d** overthrust of the hotter stack of rocks above the Andrelândia Nappe, that is, its metamorphic peak. *SFC* São Francisco Craton, *AN* Andrelândia Nappe, *LN* Liberdade Nappe, *TPVN* Três Pontas-Varginha Nappe, *SGN* Socorro-Guaxupé Nappe, *S* Suture point. See text for discussion

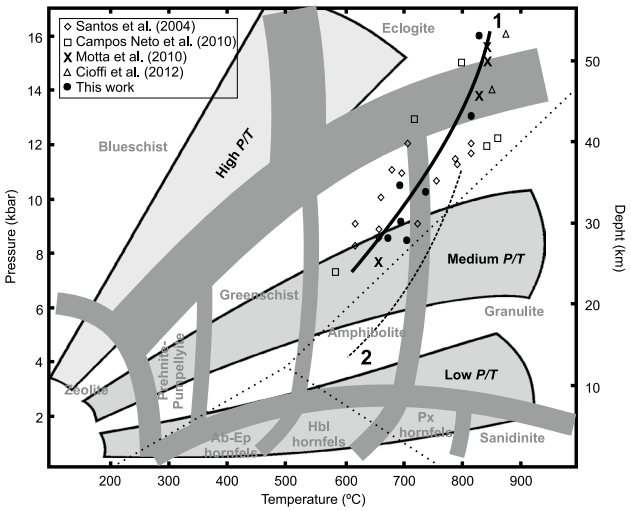

Fig. 10 Metamorphic field gradient. In *curve 1*, the Andrelândia Nappe System has the same slope as the Greater Himalayas (Fraser et al. 2000; Vannay and Hodges 1996), whereas in *curve 2*, it shows an increase in pressure and temperature between the high *P*/*T* and medium *P*/*T* series in Winter (2001)

and melanosome developed parallel to the main foliation, demonstrating that the rocks underwent partial melting and suggesting a normal metamorphic pattern. The staurolite-out and melt-in isograds are probably coincident and are parallel to the main foliation and geological contact. In the Serra da Natureza Klippe, the metamorphic peak paragenesis is composed of rutile, orthoclase, kyanite, garnet, and quartz, typical of high-pressure granulite facies conditions. These conditions were attained with the rock moving out of staurolite stability field, with muscovite and biotite melting reactions crossing inside the kyanite field, leading to

the metamorphic peak and the subsequent near-isothermal decompression *P–T* path crossing the sillimanite stability field.

The beginning of the tectono-metamorphic progression of the Andrelândia Nappe System occurred following the closure of the Goianides Ocean, with subduction of the continental crust leading to the metamorphic peak in its mid-section, which is represented by the Liberdade Nappe, at 622 Ma. Higher pressure and temperature rocks of the Serra da Natureza Klippe reached their peaks slightly later, as the isothermal relaxation was able to bring these rocks to their metamorphic peak at 604 Ma, that is, 18 Ma later. With the migration of the orogenic front, as previously proposed (Campos Neto et al. 2004), the whole stack of rocks of the Liberdade Nappe and Serra da Natureza Klippe was emplaced to shallower crustal levels, overthrusting the rocks of the Andrelândia Nappe, which achieved a metamorphic peak at 586 Ma, thereby producing an inverted metamorphic pattern. This scenario is compatible with extrusion by synconvergent ductile flow models with the folding of isotherms due to the emplacement of a cold and rigid indenter block related to rocks of the São Francisco Craton. The Andrelândia Nappe System metamorphic field gradient is consistent with that established for the rocks of the Himalayas, although the pressure and temperature are higher (i.e., between high and medium *P*/*T* series).

Acknowledgements This work was financially supported by the São Paulo Research Foundation-FAPESP (Grant 04/09682-8 and 13/04007-0). R. G. Motta is thankful to the National Counsel of Technological and Scientific Development-CNPq for the scholarship. The authors thank Marcos Mansueto for his help at the Microprobe Laboratory of Geosciences Institute-São Paulo University (USP) and Dr. Lucelene Martins for her help with the monazite analyses. Careful review of an earlier draft of this manuscript was conducted by Rebecca Jamieson, which greatly improved the final version.

References

Andreasson PG, Lagerblad B (1980) Occurrence and significance of inverted metamorphic gradients in the western Scandinavian Caledonides. J Geol Soc Lond 137:219–230. doi:10.1144/gsjgs.137.3.0219

Barbey P (2007) Diffusion-controlled biotite breakdown reaction textures at the solid/liquid transition in the continental crust. Contrib Miner Petrol 154:707–716. doi:10.1007/s00410-007-0220-x

Beaumont C, Nguyen MH, Jamieson RA, Ellis S (2006) Crustal flow modes in large hot orogens. Geol Soc Lond Spec Publ 268:91–145. doi:10.1144/GSL.SP.2006.268.01.05

Bohlen SR, Wall VJ, Boettcher AL (1983) Experimental investigations and geological applications of equilibria in the system FeO–TiO_2–Al_2O_3–SiO_2–H_2O. Am Miner 68:1049–1058

Campos Neto MC, Caby R (1999) Neoproterozoic high-pressure metamorphism and tectonic constraint from the nappe system south of the São Francisco Craton, southeast Brazil. Precambrian Res 97:3–26

Campos Neto MC, Caby R (2000) Terrane accretion and upward extrusion of high-pressure granulites in the Neoproterozoic nappes of southeast Brazil†: petrologic and structural constraints. Tectonics 19:669–687

Campos Neto MC, Basei MAS, Vlach SRF, Caby R, Szabó GAJ, Vasconcelos P (2004) Migração de orógenos e superposição de orogêneses: um esboço da Colagem Brasiliana no sul do Cráton São Francisco, SE-Brasil. Geol USP Sér Cie 4:13–40

Campos Neto MC, Basei MAS, Janasi VA, Siga Jr. O, Cordani UG (2005) O Grupo Andrelândia no Sistema de Nappes Andrelândia Oriental. In: SBG (ed) Simpósio Sobre o Cráton do São Francisco. Salvador, pp 143–146

Campos Neto MC, Janasi VA, Basei MAS, Siga Jr. O (2007) Sistema de nappes Andrelândia, setor oriental†: litoestratigrafia e posição estratigráfica. Rev Bras Geociê 37:47–60

Campos Neto MC, Cioffi CR, Moraes R, Motta RG, Siga O Jr, Basei MAS (2010) Structural and metamorphic control on the exhumation of high-P granulites: the Carvalhos Klippe example, from the oriental Andrelândia Nappe System, southern portion of the Brasília Orogen, Brazil. Precambrian Res 180:125–142. doi:10.1016/j.precamres.2010.05.010

Cioffi CR, Campos Neto MC, Rocha BC, Moraes R, Henrique-Pinto R (2012) Geochemical signatures of metasedimentary rocks of high-pressure granulite facies and their relation with partial melting: Carvalhos Klippe, Southern Brasília Belt, Brazil. J South Am Earth Sci 40:63–76. doi:10.1016/j.jsames.2012.09.007

Cioffi CR, Campos Neto MC, Moller A, Rocha BC (2016) Paleoproterozoic continental crust generation events at 2.15 and 2.08 Ga in the basement of the southern Brasília Orogen, SE Brazil. Precambrian Res 275:176–196. doi:10.1017/CBO9781107415324.004

Fraser G, Worley B, Sandiford M (2000) High-precision geothermobarometry across the high Himalayan metamorphic sequence, Langtang Valley, Nepal. J Metamorph Geol 18:665–681. doi:10.1046/j.1525-1314.2000.00283.x

Garcia MGM, Campos Neto MC (2003) Contrasting metamorphic conditions in the Neoproterozoic collision-related Nappes south of São Francisco Craton, SE Brazil. J South Am Earth Sci 15:853–870

Garcia MGM, Campos Neto MC, Fallick AE (2003) Oxygen isotope composition and geothermometry of granulite to greenschist facies metamorphic rocks†: a study from the Neoproterozoic collision-related nappe system, south of São Francisco Craton, SE Brazil. J South Am Earth Sci 15:871–883

Gibson HD, Brown RL, Parrish RR (1999) Deformation-induced inverted metamorphic field gradients: an example from the southeastern Canadian Cordillera. J Struct Geol 21:751–767. doi:10.1016/S0191-8141(99)00051-6

Godin L, Grujic D, Law RD, Searle MP (2006) Channel flow, ductile extrusion and exhumation in continental collision zones: an introduction. Geol Soc Lond Spec Publ 268:1–23. doi:10.1144/GSL.SP.2006.268.01.01

Green DH, Lambert IB (1965) Experimental crystallization of anhydrous granite at high pressures and temperatures. J Geophys Res 70:5259–5268. doi:10.1029/JZ070i020p05259

Green DH, Ringwood AE (1967) The genesis of basaltic magmas. Contrib Miner Petrol 15:103–190. doi:10.1007/BF00372052

Harrison TM, Grove M, Lovera OM, Catlos EJ, D'Andrea J (1999) The origin of Himalayan anatexis and inverted metamorphism: models and constraints. J Asian Earth Sci 17:755–772. doi:10.1016/S1367-9120(99)00018-8

Heilbron M, Pedrosa-Soares AC, Campos Neto MC, Silva LC, Trouw RAJ, Janasi VA (2004) Província Mantiqueira. In: Mantesso-Neto V, Bartorelli A, Carneiro CDR, Brito Neves BB (eds) Geologia do Continente Sul-Americano: Evolução da obra de Fernando Flávio Marques de Almeida. Beca, São Paulo, pp 204–234

Jamieson RA, Beaumont C, Medvedev S, Nguyen MH (2004) Crustal channel flows: 2. Numerical models with implications for metamorphism in the Himalayan–Tibetan orogen. J Geophys Res 109:1–24. doi:10.1029/2003JB002811

Jamieson RA, Beaumont C, Nguyen MH, Culshaw NG (2007) Synconvergent ductile flow in variable-strength continental crust: numerical models with application to the western Grenville orogen. Tectonics 26:1–23. doi:10.1029/2006TC002036

Jamieson RA, Beaumont C, Warren CJ, Nguyen M (2010) The Grenville Orogen explained? Applications and limitations of integrating numerical models with geological and geophysical data. Can J Earth Sci 47:517–539. doi:10.1139/E09-070

Jamieson RA, Unsworth MJ, Harris NBW, Rosenberg CL, Schulmann K (2011) Crustal melting and the flow of mountains. Elements 7:253–260. doi:10.2113/gselements.7.4.253

Kretz R (1983) Symbols for rock-forming minerals. Am Miner 68:277–279

Ludwig KR (2003) Isoplot 3.00: a geochronological toolkit for Microsoft Excel. Berkeley Geochronology Center Special Publication No. 4, Berkeley, 70 p

Martinez RB (2015) Avaliação de métodos para cálculo e inferência de condições P–T em rochas da fácies granulito: Investigação das rochas das Nappes Três Pontas-Varginha e Socorro-Guaxupé. Dissertation, Universidade de São Paulo

Martins L, Vlach SRF, Janasi VA (2009) Reaction microtextures of monazite: Correlation between chemical and age domains in the Nazaré Paulista migmatite, SE Brazil. Chem Geol 261:271–285. doi:10.1016/j.chemgeo.2008.09.020

Motta RG, Moraes R, Trouw RAJ, Campos Neto MC (2010) Reconstrução e comparação de trajetórias P–T no Sistema de Nappes Andrelândia, Sul da Faixa Brasília, MG. Geol USP Sér Cie 10:79–96

Mottram CM, Warren CJ, Regis D, Roberts NMW, Harris NBW, Argles TW, Parrish RR (2014) Developing an inverted Barrovian sequence; insights from monazite petrochronology. Earth Planet Sci Lett 403:418–431. doi:10.1016/j.epsl.2014.07.006

O'Brien PJ, Rotzler J (2003) High-pressure granulites: formation, recovery of peak conditions and implications for tectonics. J Metamorph Geol 21:3–20. doi:10.1046/j.1525-1314.2003.00420.x

Pitra P, Ballèvre M, Ruffet G (2010) Inverted metamorphic field gradient towards a Variscan suture zone (Champtoceaux Complex, Armorican massif, France). J Metamorph Geol 28:183–208. doi:10.1111/j.1525-1314.2009.00862.x

Powell R, Holland T (1990) Calculated mineral equilibria in the pelite system, KFMASH (K_2O–FeO–MgO–Al_2O_3–SiO_2–H_2O). Am Miner 75:367–380

Powell R, Holland T (1994) Optimal geothermometry and geobarometry. Am Miner 79:120–133

Powell R, Holland T, Worley B (1998) Calculating phase diagrams involving solid solutions via non-linear equations, with examples using THERMOCALC. J Metamorph Geol 16:577–588. doi:10.1111/j.1525-1314.1998.00157.x

Reno BL, Piccoli PM, Brown M, Trouw RAJ (2012) In situ monazite (U–Th)–Pb ages from the Southern Brasília Belt, Brazil: constraints on the high-temperature retrograde evolution of HP granulites. J Metamorph Geol 30:81–112. doi:10.1111/j.1525-1314.2011.00957.x

Santos LP, Campos Neto MC, Grohmann CH (2004) Metamorphic path constrained by metapelitic rocks from the inner Aiuruoca-Andrelândia nappe, south of the São Francisco craton, SE Brazil. J South Am Earth Sci 16:725–741. doi:10.1016/j.jsames.2003.12.006

Sawyer EW (2008) Atlas of migmatites, 9th edn. NRC Research Press, Ottawa

Searle MP, Rex AJ (1989) Thermal model for the Zanskar Himalaya. J Metamorph Geol 7:127–134. doi:10.1111/j.1525-1314.1989.tb00579.x

Simões LSA, Valeriano CM, Zanardo A, Morales N, Gomi C, Moraes R (1988) Zonação metamórfica inversa do Grupo Araxá/Canastra na região de São Sebastião do Paraíso—Alpinópolis. In: 35° Congresso Brasileiro de Geologia. SBG, Belém, pp 1203–1216

Spear FS, Cheney JT (1989) A petrogenetic grid for pelitic schists in the system SiO_2–Al_2O_3–FeO–MgO–K_2O–H_2O. Contrib Miner Petrol 101:149–164. doi:10.1007/BF00375302

Spear FS, Kohn MJ, Cheney JT (1999) *P–T* paths from anatectic pelites. Contrib Miner Petrol 134:17–32

Tomkins HS, Powell R, Ellis DJ (2007) The pressure dependence of the zirconium-in-rutile thermometer. J Metamorph Geol 25:703–713. doi:10.1111/j.1525-1314.2007.00724.x

Trouw RAJ, Ribeiro A, Paciullo FVP (1983) Geologia estrutural dos Grupos São João del Rei, Carrancas e Andrelândia, Sul de Minas Gerais. An Acad Bras Cienc 55:71–85

Trouw RAJ, Heilbron M, Ribeiro A, Valeriano CM, Almeida JCH, Tupinambá M, Andreis RR (2000a) The central segment of the Ribeira Belt. In: Cordani UG, Milani E, Thomaz Filho A, Campos DA (eds) Tectonic evolution of South America. Rio de Janeiro, pp 287–310

Trouw RAJ, Ribeiro A, Paciullo FVP, Heilbron M (2000b) Interference between the Neoproterozoic Brasilia and Ribeira Belts, with special emphasis on high-pressure granulites. In: International geological congress. Rio de Janeiro, p 45p

Trouw RAJ, Trouw CC, Peternel R, Tohver E (2008) Novas idades SHRIMP de zircões da zona de interferência entre as Faixas Brasília e Ribeira. In: 44° Congresso Brasileiro de Geologia. SBG, Curitiba, p 29

Vannay JC, Grasemann B (2001) Himalayan inverted metamorphism and syn-convergence extension as a consequence of a general shear extrusion. Geol Mag 138:253–276

Vannay JC, Hodges KV (1996) Tectonometamorphic evolution of the Himalayan metamorphic core between the Annapurna and Dhaulagiri, central Nepal. J Metamorph Geol 14:635–656

Vernon RONH (1999) Quartz and feldspar microsructures in metamorphic rocks. Can Miner 37:513–524

Vielzeuf D, Holloway JR (1988) Experimental determination of the fluid-absent melting relations in the pelitic system. Contrib Miner Petrol 98:257–276

Vielzeuf D, Montel JM (1994) Partial melting of metagreywackes. Part I. Fluid-absent experiments and phase relationships. Contrib Miner Petrol 117:375–393. doi:10.1007/BF00307272

Vlach SRF (2010) Th–U–Pb_T dating by electron microanalysis, Part I. Monazite: analytical procedures and data treatment. Geol USP Sér Cie 10:61–85

Vlach SRF, Gualda GAR (2000) Microprobe monazite dating and the ages of some granitic and metamorphic rocks from southeastern Brazil. Rev Bras Geociê 30:214–218

Warren CJ, Beaumont C, Jamieson RA (2008) Deep subduction and rapid exhumation[†]: role of crustal strength and strain weakening in continental subduction and ultrahigh-pressure rock exhumation. Tectonics 27:1–28. doi:10.1029/2008TC002292

Waters DJ (2001) The significance of prograde and retrograde quartz-bearing intergrowth microstructures in partially melted granulite-facies rocks. Lithos 56:97–110. doi:10.1016/S0024-4937(00)00061-X

Westin A (2008) Influência da pilha de nappes na trajetória metamórfica da nappe Andrelândia, borda sul do cráton São Francisco. Monograph, Universidade de São Paulo

Winter JD (2001) An introduction to igneous and metamorphic petrology. Prentice-Hall, New Jersey

Zack T, Moraes R, Kronz A (2004) Temperature dependence of Zr in rutile: Empirical calibration of a rutile thermometer. Contrib Miner Petrol 148:471–488. doi:10.1007/s00410-004-0617-8